Published for SISSA by Springer

Received: June 25, 2025
Accepted: September 15, 2025
Published: October 27, 2025

Double neutral-current corrections to NLO electroweak leptonic cross sections

Stefano Frixione,[a] **Fabio Maltoni**,[b,c,d] **Davide Pagani**[d] **and Marco Zaro**[e,f]

[a] *INFN, Sezione di Genova, Via Dodecaneso 33, Genoa, I-16146 Italy*
[b] *Centre for Cosmology, Particle Physics and Phenomenology (CP3), Université Catholique de, Louvain, Louvain-la-Neuve, B-1348 Belgium*
[c] *Dipartimento di Fisica e Astronomia, Università di Bologna, Via Irnerio 46, Bologna, I-40126 Italy*
[d] *INFN, Sezione di Bologna, Via Irnerio 46, Bologna, I-40126 Italy*
[e] *INFN, Sezione di Milano, Via Celoria 16, Milano, I-20133 Italy*
[f] *TIFLab, Università degli Studi di Milano, Via Celoria 16, Milano, I-20133 Italy*

E-mail: Stefano.Frixione@cern.ch, fabio.maltoni@uclouvain.be, davide.pagani@bo.infn.it, marco.zaro@unimi.it

Abstract: We present a method for improving next-to-leading order electroweak (EW) predictions for lepton-scattering processes by consistently including double neutral-current corrections arising from vector-boson-fusion topologies, which are formally of higher order. By combining, in a process-independent manner, exact fixed-order results, collinear resummation of QED radiation, and a subtraction procedure, we obtain results which are gauge invariant and valid in the entire phase space, retain any dependence on the masses of electroweak bosons, and can be systematically improved, while avoiding the need for complete next-to-next-to-leading order calculations. This paper is devoted to the development and validation of the formalism; phenomenological applications are presented in a companion study, where we also discuss and motivate why our approach is superior to the one based on EW parton distribution functions for targeting percent-level precision at multi-TeV lepton colliders.

Keywords: Higher Order Electroweak Calculations, Higher-Order Perturbative Calculations

ArXiv ePrint: 2506.10732

https://doi.org/10.1007/JHEP10(2025)224

JHEP10(2025)224

Contents

JHEP10(2025)224

1 Introduction

Lepton colliders have always been regarded as precision machines, where the discovery of new phenomena may happen only through a very careful comparison between measurements and the corresponding theoretical predictions. This viewpoint is informed by the fact that, historically, all lepton machines ever built have been essentially low-energy colliders, operating at energies of the order of or lower than the EW scale, whose main characteristic is that the overwhelming majority of the collisions are initiated by the annihilation of the two incoming leptons, and produce low-multiplicity final states.

In view of the fact that the high-energy physics community is presently considering the post-LHC strategy, it is useful to regard the behaviour of lepton colliders that we have just mentioned as an almost accidental by-product of two facts, in the context of a description that can be applied to both hadron and lepton collisions. Such a description

is given by the factorisation theorem,[1] which represents each incoming particle as a set of collinear partons, which predominantly collide in pairs in an incoherent manner, and whose longitudinal momentum fraction (z) distributions are given by pre-computed (or measured) functions, the Parton Distribution Function (PDFs). The two facts we have alluded to before are: *a)* the set of partons within a lepton is dominated by a lepton of the same flavour as that of the incoming one, with its PDF almost equal to a $\delta(1-z)$ (i.e. that parton carries away almost all of the momentum of the incoming particle); *b)* lepton collisions are initiated by QED and weak interactions; hence, they tend to favour low-multiplicity final states. In hadronic collisions, the almost polar opposite happens: PDFs are peaked at small-z values; and QCD drives the hard reactions, thus rendering it easy to find high-multiplicity final states.

As was mentioned before, this dichotomy between lepton and hadron colliders is an accident due to the low-energy nature of the former. In fact, by increasing the centre-of-mass energy (c.m. henceforth), a lepton collider gradually acquires the characteristics typical of a hadron collider. In particular, one starts to see that the peaks of the transverse momenta tend to move from the high-end of the spectrum towards small values; likewise for the invariant masses of the systems of objects tagged in the final state. Technically, this happens because large energies mean the possibility of probing parton contents at smaller z values, where one is not dominated any longer by lepton PDFs, but rather by those of the photon and, increasingly, of the gluon and of the quarks. Furthermore, phase spaces associated with larger multiplicities become sizeable, hence in part offsetting the suppression due to the QED/weak coupling constant factors.

The increase of the collider energy therefore results in a richer set of phenomena, and in new discovery strategies.[2] In particular, in the context of muon-collider studies, the class of vector boson fusion (VBF henceforth) processes has received a significant amount of attention, in view of its becoming one of the dominant production mechanisms at high c.m. energies; this fits nicely with the fact that, theoretically, the vector bosons exchanged in the t channels can effectively be treated as partons within the incoming leptons, i.e. as *massless* objects associated with a PDF. While one can prove that all of the contributions neglected by this approximation vanish with the c.m. energy that goes to infinity, the speed at which one approaches such a limit is logarithmic; therefore, for realistic collider configurations, with energies in the range of a few TeVs or even tens of TeVs, the neglected contributions may still be important, and even dominant. When this is the case, one sees that VBF processes are not even well-defined quantities, but merely denote a subset of the Feynman diagrams that contribute to the production of the system of interest (e.g. a Higgs, a W^+W^- pair, and so forth). This implies that, in order to carry out studies which are guaranteed to be unbiased theoretically, one must have predictions that are correct in the whole phase space, thus being able to describe both the regions where VBF kinematic configurations are important, and

[1] For a recent review on this and its alternatives which focuses on e^+e^- physics, see e.g. [1].

[2] It is important to note that, in large part, the problems and opportunities associated with an energy increase are the same as those one is confronted with when the goal is to reach extremely high precision. In other words, the discussions about a 10 TeV muon colliders with a percent-level program will touch many of the issues relevant to a 500 GeV electron machine which aims at measuring a few observables with a relative precision of, say, 10^{-5} — an example of particular relevance for this paper is the impact of the $\gamma\gamma$-fusion channel.

JHEP10(2025)224

those where they are negligible, with a seamless transition between the two; an important component of this is the ability to control the theoretical uncertainties.

The approach where EW vector bosons are regarded as massless partons within the incoming lepton does not fulfill this requirement. The solution, in itself or as a starting point for further refinements, is the perturbative computation of the cross section of interest that features all of the relevant contributions, including but not limited to VBF topologies. The problem with such a solution is that calculations increase sharply in complexity with the perturbative order. While this is directly relevant to VBF topologies, since these are suppressed by the square of the coupling constant w.r.t. Born contributions[3] (i.e. are of next-to-next-to-leading order (NNLO)), it is fortunately the case that VBF graphs are simple to compute — they are tree-level ones, with a straightforward singularity structure.

This observation is the motivation behind this work, whose goal is the inclusion of terms of NNLO, and specifically those which stem from VBF topologies, in perturbative predictions whose accuracy is of next-to-leading order (NLO), without performing complete NNLO calculations, but in a gauge-invariant manner, and by retaining the exact dependences on vector boson masses and the capability of firmly assessing the theoretical systematics.

This paper is organised as follows. We introduce the problem and discuss some general issues in section 2. We present the core part of the procedure in section 3. The resulting formula cannot be used as is in order to obtain physical predictions, and we expose its limitations and scope in section 4. We then proceed to lift such limitations in section 5, and arrive at the final result in section 6. We conclude in section 7, and collect additional material in the appendices.

This is a technical paper, whose goal is achieved by means of a sequence of formal manipulations. The reader who is interested only in the underpinning logic and in the final result can find a summary of the former in section 2, and the latter in eqs. (7.1), (7.2), and (7.3). Some immediate phenomenological consequences of our work are presented in section 6.1.1, section 6.1.2, and more extensively in a companion paper [2].

2 Generalities

We are interested in studying the properties of a system $T = \{T_1, \dots T_m\}$ of m particles produced in $\ell^+\ell^-$ collisions, with $\ell = e$ or $\ell = \mu$. We shall loosely identify the T_i's as "tagged" objects, regardless of whether they can actually be directly tagged in a detector (this happens e.g. when $T = \{e^+, e^-\}$ or $T = \{\gamma, \gamma, \gamma, \gamma\}$), or only indirectly, for example through their decay products (this is the case e.g. when $T = \{t, \bar{t}\}$ or $T = \{W^+, W^-\}$). Indeed, from a theoretical viewpoint the direct or indirect nature of the tagging is irrelevant; what matters is the ability to calculate, in a manner which we assume to be perturbative, the cross sections associated with the processes:

$$\ell^- + \ell^+ \longrightarrow T \cup U_q\,, \qquad T \cup U_q \equiv T_1 + \dots T_m + u_1 + \dots u_q\,, \tag{2.1}$$

for any set $U_q = \{u_1, \dots u_q\}$ of q particles that may be taggable or not, but that we generally regard as *not* tagged in the context of our experiment: thus, we call them "untagged". Roughly

[3] Barring accidental zeros at the Born level; however, when such zeros are present, the cross section remains small in absolute value, still owing to the suppression by the coupling constant.

JHEP10(2025)224

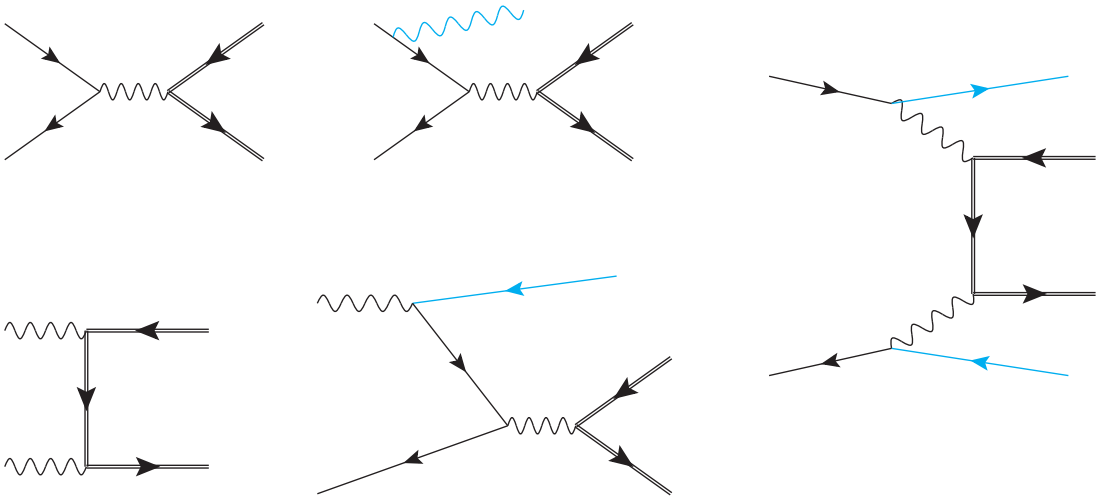

Figure 1. Representative tree-level $t\bar{t}$-production diagrams at the level of short-distance cross sections, of order $\alpha^2\alpha^0$ (left panel, $\ell^+\ell^-$ and $\gamma\gamma$ channels), $\alpha^2\alpha^1$ (middle panel, $\ell^+\ell^-$ and $\gamma\ell$ channels), and $\alpha^2\alpha^2$ (right panel, $\ell^+\ell^-$ channel only).

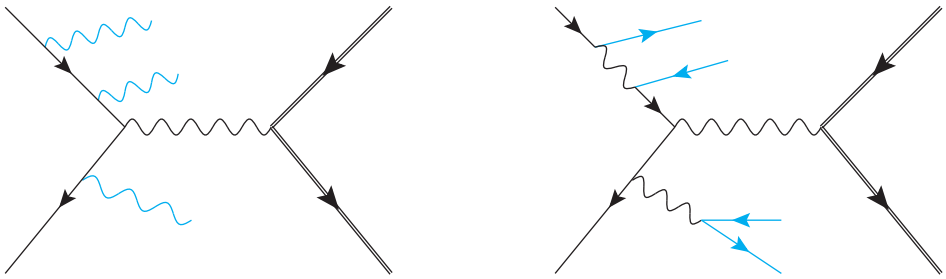

Figure 2. Representative tree-level $t\bar{t}$-production diagrams of order $\alpha^2\alpha^3$ (left panel) and $\alpha^2\alpha^4$ (right panel).

speaking, the cross section associated with eq. (2.1) will be proportional, in a fixed-order perturbative approach, to a coupling-constant factor[4]

$$\alpha^b\alpha^q\,, \tag{2.2}$$

having denoted by α the coupling constant of the theory we are working with (i.e. typically the EW sector of the SM), and by b an integer characteristic of the production of the sole system T.

In order to be definite, let us consider the case of $t\bar{t}$ production. Sample perturbative diagrams for the production of this tagged system are depicted in figures 1 and 2. There, we have represented as thick black lines the t and the $\bar{t}$ quarks, and as blue lines the untagged particles. In reference to eq. (2.2), we have $b = 2$, whilst the relevant value of q is obtained by counting the number of final-state untagged particles. The wiggly lines represent electroweak

[4]It is always possible to use eq. (2.2) when working at the tree level, while it becomes ambiguous or outright impossible when virtual corrections are involved. Here, we employ that equation *only* in order to help one understand the arguments of this section in an intuitive manner. Furthermore, we ignore the contributions due to strongly-interacting particles in either the initial or the final state; that said, our formalism will require no modifications should one wish to include them.

JHEP10(2025)224

vector bosons, including W's in the case of the rightmost panel of figure 1 (when this happens, the t-channel fermion line actually represents a b quark, whereas the two outgoing fermion lines represent neutrinos).

The calculation of the matrix elements that correspond to the graphs above increase in complexity with the overall power of α; there is both a technical complexity stemming from each graph, and a bookkeeping complexity due to the growth of the number of diagrams. The problem becomes rapidly so severe that one must resort to some kind of approximation — for example, the diagrams of figure 2 are typically replaced by the diagrams in the leftmost panel of figure 1, whose matrix elements are then convoluted with the so-called Parton Distribution Functions (PDFs), which account for any number of *collinear* emissions of any types of particles (whence the necessity of including contributions where the initial state is *not* an $\ell^+\ell^-$ one,[5] as in the graphs at the bottom of the left and middle panels of that figure). In the notation introduced before, the PDFs are an effective way to sum over *all* sets U_q, with $0 \leq q \leq \infty$, provided that all of the particles in such sets are emitted collinearly to the incoming lines.

An unavoidable consequence of employing an approximation based on PDFs is that any information on the masses of the particles involved in the corresponding collinear process is solely constituted by the arguments of logarithms, which are equal to the ratios of such masses over a hard scale that characterises the process (e.g. the invariant mass of the tagged system T). Specifically, the information is lost on the behaviour of the cross section as a function with polynomial- or square-root-type dependence on these masses (henceforth, we shall call this behaviour "power-suppressed effects"). This is not a particularly steep price to pay if the particles in question are photons or light leptons, whose masses are already null or negligible, and the use of PDFs is in fact helpful in keeping the logarithmic growth of the cross section under control. The situation is manifestly very different if one considers Z and W bosons, whose masses are hardly negligible but at asymptotically-high energies. By far and large, this strongly hints at the fact that the uncertainties due to neglecting such masses in simulations relevant to *any collider configurations ever considered to be realistic* are possibly very significant. In particular, power-suppressed effects are expected to be dominant or fairly large in a sizeable part of the phase space. In general, the reasons for questioning the accuracy of PDF approaches that involve weak bosons (called EW PDFs henceforth), such as those of refs. [3, 4], are related to the following issues.

- Results obtained by means of exact matrix element computations exhibit large differences w.r.t. those emerging from the so-called Effective Weak-boson Approximation (EWA), in the absence of observable-specific fine tunings of the scale parameters that enter the latter (see ref. [2]). One needs to bear in mind that an EWA approach relies on functions which can be regarded as the first-order expansions[6] of the corresponding EW PDFs (or, equivalently, as the initial conditions for their evolution).

[5] While the identities of the initial-state particles at the short-distance level may be different from those of the beam particles, we always regard the mechanism which produces them as perturbative, as opposed to multi-particle phenomena such as beamstrahlung, with which we are not concerned in this work.

[6] This condition may be relaxed, and thus *some* power-suppressed effects can be included in the EWA even at the LO. While this improves the agreement with matrix-element predictions, it further degrades the control on the theoretical uncertainties associated with the EWA.

JHEP10(2025)224

- The differences between EW-PDF- and EWA-induced results are smaller than the (very large) uncertainties associated with the approximations that these methods entail. This fact, and the previous item, imply that all-order resummation effects, included in the EW PDFs but absent in the EWA, are subdominant w.r.t. to the differences that either of these predictions (if not fine-tuned) have in comparison to matrix-element-based results, which are relevant precisely because resummation is not necessary.

- The uncertainties inherent in the EW PDFs and EWA approaches are in part not parametric in nature (i.e. they do not scale with powers of the vector boson masses or the coupling constants), and thus cannot be assessed in a fully reliable manner.

- Being equivalent to a massless approach, EW-PDF- and EWA-based computations lack any description of power-suppressed effects [6]; therefore, we expect them to be unreliable in particular at and near the threshold region, where any agreement with the correct result is accidental, except in the cases where the typical scale of the produced system is much larger than the EW scale.

- Current EW PDFs are leading-logarithmic (LL) and leading-order (LO) accurate (contrary to their light-particle counterparts). As a consequence of this, short-distance cross section predictions are beyond accuracy if they include contributions of next-to-leading order (NLO) or higher.

- It follows from the previous item that the usage of (LL and LO) EW PDFs implies that only a subset of the diagrams relevant to a given process can be considered: the effects of the remaining diagrams are neglected, and their impact cannot be estimated.

- It then further follows that, since simulations with EW PDFs are fully inclusive in the particles that emerge from the boson branchings and one can only use LO matrix elements, such simulations implement a much simpler kinematic structure than that of the processes they are meant to approximate. This may pose serious difficulties when one tries to reproduce the typical experimental setup; for example, certain observables are impossible to define, trivial, or over-simplified.

For these reasons, it seems wise to develop a rigorous approach based on exact matrix element calculations whenever massive vector bosons are involved. In this context, there are two main obstacles, namely: *a)* the computations are technically demanding; *b)* a strict matrix element approach cannot work well when photons and light leptons are also present, since logarithmic effects associated with such particles are not resummed, and they must be — as we shall see, the solution entails using both massive matrix elements and PDFs associated with light objects.

A situation where either or both of these drawbacks are relevant is that represented by the VBF-like graph in the rightmost panel of figure 1, which is indeed the case most often cited as *the* reason for employing an EW-PDF approach. Preliminarily, let us remark that the set of such graphs constitutes, from a perturbative viewpoint, a single class of the much larger set of all of the NNLO diagrams, which are suppressed by two powers of the coupling constant w.r.t. the leading-order (LO) contributions. Therefore, for the VBF-like topologies to be dominant, one must be in a rather special kinematical configuration where

JHEP10(2025)224

both the coupling-constant suppression and the competition from other NNLO graphs are overcome. Clearly, complete NNLO results would render both points moot, but such results are indeed very difficult to obtain at present. One can therefore limit oneself to considering all double-real tree-level graphs. This bypasses a significant fraction of the technical difficulties, but the one associated with the fixed-order treatment of massless-particle branching remains, for those processes that feature both Z and γ exchanges.

The formalism we shall derive in the remainder of this paper is such that:

- It uses all of the exact matrix-elements of LO and NLO, as well as those associated with all of the $\ell^+\ell^-$-initiated double-real graphs of NNLO, for all particles involved, be them massive, nearly-massless, or massless.
- It includes the resummation of small-mass effects by using lepton, photon and, if necessary, quark and gluon PDFs, at the accuracy at which such PDFs are available (presently, next-to-leading logarithmic [5–7]).
- It smoothly matches the two (i.e. hard and collinear) regimes, so that no information is lost anywhere in the phase space, and the energy range can be scanned from the threshold region to the collider energy at the same level of accuracy.
- It allows one to include further improvements, such as the inclusion of Sudakov-resummed results and of higher-order corrections for those channels which open up at the NNLO.

The key for achieving these objectives is a careful treatment of VBF-like diagrams, which we shall discuss in the next section.

In conclusion, a remark about notation. In view of the fact that this point is generally ambiguous, we specify that by NLO and NNLO we understand a prediction at that level of accuracy — that is, in reference to eq. (2.2), NLO corresponds the *sum* of the $\mathcal{O}(\alpha^b)$ and the $\mathcal{O}(\alpha^{b+1})$ contributions, while NNLO is the NLO result *plus* the $\mathcal{O}(\alpha^{b+2})$ contributions. Conversely, by δNLO and δNNLO we understand the sole *corrections*, i.e. the $\mathcal{O}(\alpha^{b+1})$ and $\mathcal{O}(\alpha^{b+2})$ contributions, respectively. In addition to that, the LO, (δ)NLO, and (δ)NNLO contributions that we specifically address in this paper are denoted by LO_Γ, (δ)NLO_Γ, and (δ)NNLO_Γ, respectively. In the case of the LO, LO_Γ coincides with the results of the $\gamma\gamma$-initiated process, and can thus be denoted by $\text{LO}_{\gamma\gamma}$ as well.

3 VBF-like configurations with electroweak vector bosons

We shall assign the kinematics of any $2 \to 2 + m$ process thus including, but being not limited to, a VBF-like one, as follows:

$$\ell^-(p_1) + \ell^+(p_2) \longrightarrow T + \ell^-(k_1) + \ell^+(k_2)\,, \tag{3.1}$$

having used the same notation as in eq. (2.1), with the untagged particles explicitly chosen to be leptons of the same flavour as that of the incoming ones. As was said in section 2, we are specifically interested in the contributions to the process of eq. (3.1) due to VBF topologies that feature both Z and γ exchanges. Absent hard cuts on the outgoing leptons, there will

JHEP10(2025)224

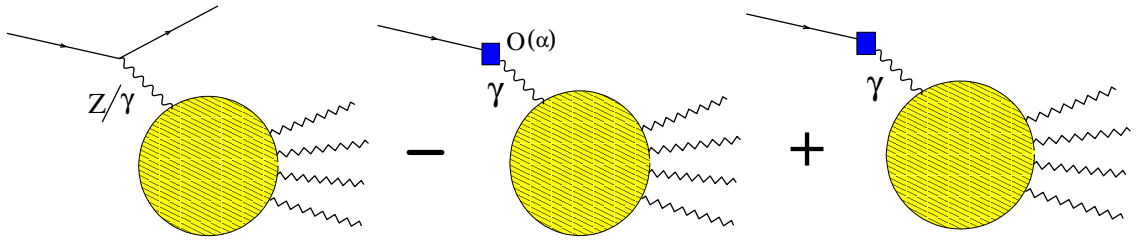

Figure 3. Upper half of a VBF configuration in $\ell^+\ell^-$ collisions; for brevity, only one side of the Cutkosky diagrams is shown. Left panel: exact matrix elements. Middle panel: with $\mathcal{O}(\alpha)$ expansion of the γ PDF. Right panel: with the full γ PDF.

be a phase-space region where the cross section is dominated by kinematical configurations with such leptons collinear to the incoming ones. In fact, if the leptons are assumed to be massless, the matrix elements that feature photon exchanges are divergent in the collinear limit; with massive leptons, the matrix elements are dominated by $\log Q^2/m^2$ terms, with Q the typical hard scale of the process and m the lepton mass; in all relevant scenarios, power-suppressed effects associated with the lepton mass ($(m^2/Q^2)^c$ for some $c > 0$) are negligible. Conversely, both logarithmic ($\log Q^2/m_Z^2$) and power-suppressed ($(m_Z^2/Q^2)^d$ for some $d > 0$, not necessarily equal to c) effects due to the Z boson need to be retained.

We start by pointing out that the procedure we are going to define works also for one "VBF vertex" at a time; thus, we can concentrate, say, on the upper half of the VBF diagram, and subsequently apply our results to the bottom half. This has the advantage that the procedure can be applied to any kind of process that features at least one Z-boson t-channel exchange, a class larger than, but which includes, the VBF processes. Thus, we begin by considering the process[7]

$$\ell^-(p_1) + a(p_2) \longrightarrow (Z/\gamma)^* \longrightarrow \ell^-(k_1) + X \tag{3.2}$$

rather than that of eq. (3.1); this is symbolically depicted in the left panel of figure 3 (where we omit particle a). By assuming the system X to be made of n particles,[8] we write the cross section for the process of eq. (3.2) as follows:

$$d\bar{\sigma}_\ell^{(n+1)} = \overline{\mathcal{M}}_\ell^{(n+1)} d\phi_{n+1}\,, \tag{3.3}$$

with $\overline{\mathcal{M}}_\ell^{(n+1)}$ the matrix element computed with massive leptons (hence the overline, following the notational conventions of ref. [8]). The basic idea of the procedure that follows is this:

- Add to the matrix element of eq. (3.3) (the square of the graph in the leftmost panel of figure 3) a quantity which is equal to zero at $\mathcal{O}(\alpha)$, given by the difference of the reduced cross section convoluted with the photon PDF (the square of the graph in the rightmost panel of figure 3) minus the same thing expanded at $\mathcal{O}(\alpha)$, supplemented by collinear remainders of matrix-element origin (the square of the graph in the middle panel of figure 3).

[7] Here and elsewhere, the intermediate $(Z/\gamma)^*$ notation reminds one that such vector bosons *may* be exchanged in the t channel(s); however, the matrix elements always include all contributions.

[8] While from eq. (3.1) we have $a = \ell^+$, $X = \{\ell^+(k_2), T\}$ and $n = m + 1$, eq. (3.2) and its subsequent manipulations do not rely on these relationships.

JHEP10(2025)224

In order to do this, we must compute the leading behaviour of eq. (3.3) in the collinear configuration $p_1 \parallel k_1$. From eq. (**I**.5.15):[9]

$$\overline{\mathcal{M}}_\ell^{(n+1)} \overset{p_1\parallel k_1}{\longrightarrow} \frac{e^2}{p_1\cdot k_1 - m^2} P^<_{\gamma^\star \ell}(z)\, \mathcal{M}_\gamma^{(n)}(zp_1)\,. \tag{3.4}$$

The massive-lepton Altarelli-Parisi kernel can be found in appendix B of ref. [8]:

$$P^<_{\gamma^\star\ell}(z) = \frac{1+(1-z)^2}{z} - \frac{z\,m^2}{p_1\cdot k_1 - m^2}\,. \tag{3.5}$$

The matrix element $\mathcal{M}_\gamma^{(n)}(zp_1)$ is the one relevant to the process:

$$\gamma(zp_1) + a(p_2) \;\longrightarrow\; X\,, \tag{3.6}$$

where all lepton-mass effects are neglected (i.e., $p_1^2 = 0$ in eq. (3.6): the photon is on-shell), and eq. (3.4) is understood to be valid up to terms suppressed by powers of m^2/Q^2. Equation (3.4) follows from the usual argument of collinear dominance; the reduced n-body matrix element that factorises features only the photon (and not the Z), since a collinearly-divergent Feynman graph (which is only associated with photon exchange) must appear on both sides of the cut to give a leading $1/k_\perp^2$ behaviour.

For the explicit computation of eq. (3.4) we parametrise the relevant momenta as follows:

$$p_1 = (E_1, 0, 0, p)\,, \qquad E_1 = \sqrt{m^2+p^2}\,, \tag{3.7}$$

$$k_1 = \frac{\sqrt{s}}{2}\,\xi\left(1, \vec{e}\sqrt{1-y^2}\,\beta_k, y\,\beta_k\right)\,, \tag{3.8}$$

where, having defined $s = (p_1+p_2)^2$ and $m_2^2 = p_2^2$:

$$E_1 = \frac{\sqrt{s}}{2}\left(1 + \frac{m^2-m_2^2}{s}\right)\,, \tag{3.9}$$

$$p = \frac{\sqrt{s}}{2}\sqrt{1-\frac{(m+m_2)^2}{s}}\sqrt{1-\frac{(m-m_2)^2}{s}}\,, \tag{3.10}$$

$$\beta_k = \sqrt{1-\frac{4m^2}{s\,\xi^2}}\,. \tag{3.11}$$

This parametrisation is the standard FKS [9, 10] one, where one works in the c.m. frame of the incoming particles. As usual, we identify $\xi = 1-z$, z being that which appears in eq. (3.4). In practice, we are interested in the two cases $m_2 = m$ and $m_2 = 0$, which correspond to $a \equiv \ell^+$ and $a = \gamma$, respectively; we shall show that these lead to the same result for eq. (3.4). The above momentum parametrisation corresponds to the following phase space (see eq. (**I**.5.21)–eq. (**I**.5.23)):

$$d\phi_{n+1}(p_1,p_2;k_1,X_1\dots X_n) = d\tilde{\phi}_n(p_1,p_2;k_1,X_1\dots X_n)\,d\phi_1(k_1)\,, \tag{3.12}$$

$$d\tilde{\phi}_n(p_1,p_2;k_1,X_1\dots X_n) = (2\pi)^4\delta\left(p_1+p_2-k_1-\sum_{i=1}^n X_i\right)\prod_{i=1}^n \frac{d^3X_i}{(2\pi)^3 2X_i^0}\,, \tag{3.13}$$

$$d\phi_1(k_1) = \frac{d^3k_1}{(2\pi)^3 2k_1^0} = \frac{1}{2(2\pi)^3}\,\frac{s\beta_k^3}{4}\,\xi d\xi\,dy\,d\varphi\,. \tag{3.14}$$

[9] Henceforth, eq. (x.y) of ref. [8] will be denoted by eq. (**I**.x.y).

JHEP10(2025)224

By means of direct computations we obtain what follows:

$$p_1\cdot k_1 - m^2 = \frac{s}{4} f \left(1 - \frac{y}{1+\rho}\right) , \tag{3.15}$$

where, if $m_2 = m$:

$$f = \xi - \frac{4m^2}{s} , \tag{3.16}$$

$$\frac{1}{1+\rho} = \frac{\xi\beta_k}{f}\sqrt{1-\frac{4m^2}{s}} \quad \Longrightarrow \quad \rho = 2\frac{(1-\xi)^2}{\xi^2}\frac{m^2}{s} + \mathcal{O}\left(\frac{m^4}{s^2}\right) , \tag{3.17}$$

while if $m_2 = 0$:

$$f = \xi\left(1+\frac{m^2}{s}\right) - \frac{4m^2}{s} , \tag{3.18}$$

$$\frac{1}{1+\rho} = \frac{\xi\beta_k}{f}\left(1-\frac{m^2}{s}\right) \quad \Longrightarrow \quad \rho = 2\frac{(1-\xi)^2}{\xi^2}\frac{m^2}{s} + \mathcal{O}\left(\frac{m^4}{s^2}\right) . \tag{3.19}$$

Importantly, this shows that the leading behaviour in m^2/s of the ρ parameter is the same in the two cases of interest; ultimately, this is due to the invariance under longitudinal boosts of massless-lepton results. By using these formulae and the distributions identities in eq. (**I**.4.108) and eq. (**I**.4.182), namely:

$$\begin{aligned}\frac{1}{\left(1\pm\frac{y}{1+\rho}\right)^2} = &\left(\frac{1}{\rho}+\frac{3}{2}\right)\delta(1\pm y) + \left(\log\frac{\rho}{2}+1\right)\delta'(1\pm y) \\ &+ \sum_{j=2}^{\infty}\frac{(-1)^j\,2^{j-1}}{(j-1)\,j!}\,\delta^{(j)}(1-y) + \mathcal{O}(\rho) ,\end{aligned} \tag{3.20}$$

$$\frac{1}{1-\frac{y}{1+\rho}} = -\log\frac{\rho}{2}\,\delta(1-y) + \left(\frac{1}{1-y}\right)_+ + \mathcal{O}(\rho) , \tag{3.21}$$

and by discarding terms suppressed by powers of m^2/s, we arrive at:

$$\begin{aligned}d\bar{\sigma}_\ell^{(n+1)} \overset{p_1\|k_1}{\longrightarrow} &\frac{\alpha}{2\pi}\,\mathcal{Q}_{\gamma\ell}(1-\xi)\mathcal{M}_\gamma^{(n)}\big((1-\xi)p_1\big)\,\delta(1-y)\,d\xi\,dy\,d\tilde{\phi}_n \\ &+ \frac{4e^2}{s\xi}\,\frac{1+\xi^2}{1-\xi}\left(\frac{1}{1-y}\right)_+ \mathcal{M}_\gamma^{(n)}\big((1-\xi)p_1\big)\,d\phi_{n+1} ,\end{aligned} \tag{3.22}$$

with (see eq. (**I**.4.187)):

$$\mathcal{Q}_{\gamma\ell}(1-\xi) = -\left[\frac{1+\xi^2}{1-\xi}\left(2\log\frac{1-\xi}{\xi}+\log\frac{m^2}{s}\right)+\frac{2\xi}{1-\xi}\right] . \tag{3.23}$$

From eqs. (3.4) and (3.5), we see that the expression on the second line of eq. (3.22) is, apart from the endpoint contribution of the plus distribution, the collinear limit of the massless-lepton matrix elements, $\mathcal{M}_\ell^{(n+1)}$. In the first line, the exact n-body phase space appears, since from eq. (**I**.5.24):

$$d\tilde{\phi}_n(p_1,p_2;k_1,X_1\dots X_n)\,\delta(1-y) \overset{m\to 0}{\longrightarrow} d\phi_n\big((1-\xi)p_1,X_1\dots X_n\big)\,\delta(1-y) . \tag{3.24}$$

JHEP10(2025)224

At the same level of accuracy as that of eq. (3.22), we can therefore write:

$$d\bar{\sigma}_{\ell}^{(n+1)} \overset{p_1\|k_1}{\longrightarrow} \frac{\alpha}{2\pi}\,\mathcal{Q}_{\gamma\ell}(z)\mathcal{M}_{\gamma}^{(n)}(zp_1)\,d\phi_n(zp_1)\,dz + \left(\frac{1}{1-y}\right)_+\left((1-y)\mathcal{M}_{\ell}^{(n+1)}\right)d\phi_{n+1}\,. \tag{3.25}$$

Equation (3.25) gives the collinear limit of the massive-lepton cross section in terms of the subtracted *massless*-lepton one (that features both γ and Z t-channel exchanges, as well as any other tree-level diagram of the same order), plus an n-body quantity that is the convolution of a universal kernel $\mathcal{Q}_{\gamma\ell}$ with the cross section for the γ-initiated process of eq. (3.6). Note that, owing to the subtraction, the massless-lepton cross section is finite in the collinear limit: the role of its singularity is played by the $\log m^2/s$ term which appears in $\mathcal{Q}_{\gamma\ell}$, and that corresponds to the leading behaviour of the massive-lepton cross section.

The n-body γ-initiated cross section is also what appears in the expression for the process of eq. (3.2) that emerges from collinear factorisation. This, we write as follows:

$$\begin{aligned} d\hat{\sigma}_{\gamma}^{(n)} &= \Gamma_{\gamma/\ell}(z)\,\mathcal{M}_{\gamma}^{(n)}(zp_1)\,d\phi_n(zp_1)\,dz & (3.26)\\ &= \left(\frac{\alpha}{2\pi}\Gamma_{\gamma/\ell}^{[1]}(z)+\mathcal{O}(\alpha^2)\right)\mathcal{M}_{\gamma}^{(n)}(zp_1)\,d\phi_n(zp_1)\,dz\\ &\equiv d\hat{\sigma}_{\gamma\mathcal{O}(\alpha)}^{(n)}+\mathcal{O}(\alpha^2)\,, & (3.27)\end{aligned}$$

where eq. (3.27) is simply eq. (3.26) after expanding the photon PDF at $\mathcal{O}(\alpha)$. Equations (3.26) and (3.27) are depicted in the right and middle panels, respectively, of figure 3. $\Gamma_{\gamma/\ell}^{[1]}$ can be found in eq. (**I**.4.189):

$$\Gamma_{\gamma/\ell}^{[1]}(z) = \frac{1+(1-z)^2}{z}\left(\log\frac{\mu^2}{m^2}-2\log z-1\right)+K_{\gamma\ell}(z)\,, \tag{3.28}$$

where $\mu^2\sim s$ is the mass-scale squared at which the PDF is evaluated, and $K_{\gamma\ell}(z)$ is a function that defines the factorisation scheme (see refs. [11, 12] for more details on its definition, for both LL and NLL PDFs). It is now apparent that the leading $m\to 0$ behaviours of eqs. (3.25) and (3.27) are identical (as they should by construction). This implies that:

$$\begin{aligned} d\bar{\sigma}_{\ell}^{(n+1)} &= \frac{\alpha}{2\pi}\,\mathcal{Q}_{\gamma\ell}(z)\mathcal{M}_{\gamma}^{(n)}(zp_1)\,d\phi_n(zp_1)\,dz - d\hat{\sigma}_{\gamma\mathcal{O}(\alpha)}^{(n)} & (3.29)\\ &\quad+\left(\frac{1}{1-y}\right)_+\left((1-y)\mathcal{M}_{\ell}^{(n+1)}\right)d\phi_{n+1}+d\hat{\sigma}_{\gamma}^{(n)}+\mathcal{O}\left(\alpha^2,\frac{m^2}{s}\right)\,.\end{aligned}$$

The r.h.s. of this equation is depicted symbolically in figure 3: the sought collinear-improved $(n+1)$-body cross section which features Z/γ interference is obtained as the sum of the subtracted $(n+1)$-body massless-lepton cross section, plus the convolution of the γ PDF with the n-body γ-initiated one, plus the convolution of the latter with a collinear-finite kernel, whose expression is obtained from the first line of eq. (3.29), namely:

$$\begin{aligned} &\frac{\alpha}{2\pi}\,\mathcal{Q}_{\gamma\ell}(z)\mathcal{M}_{\gamma}^{(n)}(zp_1)\,d\phi_n(zp_1)\,dz - d\hat{\sigma}_{\gamma\mathcal{O}(\alpha)}^{(n)}\\ &=\frac{\alpha}{2\pi}\,\mathcal{Q}'_{\gamma\ell}(z)\mathcal{M}_{\gamma}^{(n)}(zp_1)\,d\phi_n(zp_1)\,dz\,, \end{aligned} \tag{3.30}$$

JHEP10(2025)224

with:

$$\mathcal{Q}'_{\gamma\ell}(z) = \frac{1+(1-z)^2}{z}\left(\log\frac{s}{\mu^2}+2\log(1-z)\right)+z-K_{\gamma\ell}(z)\,. \tag{3.31}$$

Thus finally the collinear-improved expression of the original cross section is:

$$\begin{aligned}\overline{\mathcal{M}}_{\ell}^{(n+1)}d\phi_{n+1} \longrightarrow{}& \left(\frac{1}{1-y}\right)_+\left((1-y)\mathcal{M}_{\ell}^{(n+1)}\right)d\phi_{n+1}\\ &+\frac{\alpha}{2\pi}\,\mathcal{Q}'_{\gamma\ell}(z)\mathcal{M}_{\gamma}^{(n)}(zp_1)\,d\phi_n(zp_1)\,dz+d\hat{\sigma}_{\gamma}^{(n)}\,,\end{aligned} \tag{3.32}$$

with $d\hat{\sigma}_{\gamma}^{(n)}$ given in eq. (3.26). Equation (3.32) achieves formally the goal stated in the bullet point at page 8 and symbolically[10] depicted in figure 3. Loosely speaking, the first and second terms of eq. (3.32) correspond to the two leftmost panels of the figure, whereas the third term corresponds to the rightmost panel.

Now we observe that each of the cross sections that appear in eq. (3.32) may feature the same structure as the cross section we have started from, i.e. that for eq. (3.2) — in other words, they may correspond to the lower half of a VBF diagram. In that case, the procedure above should be iterated; this explains why it has been carried out for the process in eq. (3.2), rather than for the original one of eq. (3.1). In order to carry out such an iteration,[11] we start by re-writing eq. (3.32) in a more explicit manner as far as parton indices are concerned, thus:

$$\begin{aligned}\overline{\mathcal{M}}_{\ell\ell}^{(m+2)}d\phi_{m+2} \longrightarrow{}& \left(\frac{1}{1-y_1}\right)_+\left((1-y_1)\mathcal{M}_{\ell\ell}^{(m+2)}\right)d\phi_{m+2}(p_1,p_2)\\ &+\left(\Gamma_{\gamma/\ell}(z_1)+\frac{\alpha}{2\pi}\,\mathcal{Q}'_{\gamma\ell}(z_1)\right)\mathcal{M}_{\gamma\ell}^{(m+1)}\,d\phi_{m+1}(z_1p_1,p_2)\,dz_1\,,\end{aligned} \tag{3.33}$$

having renamed $z\to z_1$ and $y\to y_1$, and having employed the relationships in footnote 8. By applying the replacement of eq. (3.33) to the rightmost lepton indices that appear in each of the matrix elements in its r.h.s., we obtain what follows:

$$\begin{aligned}\overline{\mathcal{M}}_{\ell\ell}^{(m+2)}d\phi_{m+2} \longrightarrow{}& \left(\frac{1}{1-y_1}\right)_+\left(\frac{1}{1-y_2}\right)_+\left((1-y_1)(1-y_2)\mathcal{M}_{\ell\ell}^{(m+2)}\right)d\phi_{m+2}(p_1,p_2)\\ &+\left(\Gamma_{\gamma/\ell}(z_2)+\frac{\alpha}{2\pi}\,\mathcal{Q}'_{\gamma\ell}(z_2)\right)\left(\frac{1}{1-y_1}\right)_+\\ &\times\left((1-y_1)\mathcal{M}_{\ell\gamma}^{(m+1)}\right)d\phi_{m+1}(p_1,z_2p_2)\,dz_2\\ &+\left(\Gamma_{\gamma/\ell}(z_1)+\frac{\alpha}{2\pi}\,\mathcal{Q}'_{\gamma\ell}(z_1)\right)\left(\frac{1}{1-y_2}\right)_+\\ &\times\left((1-y_2)\mathcal{M}_{\gamma\ell}^{(m+1)}\right)d\phi_{m+1}(z_1p_1,p_2)\,dz_1\\ &+\left(\Gamma_{\gamma/\ell}(z_1)+\frac{\alpha}{2\pi}\,\mathcal{Q}'_{\gamma\ell}(z_1)\right)\left(\Gamma_{\gamma/\ell}(z_2)+\frac{\alpha}{2\pi}\,\mathcal{Q}'_{\gamma\ell}(z_2)\right)\\ &\times\mathcal{M}_{\gamma\gamma}^{(m)}\,d\phi_m(z_1p_1,z_2p_2)\,dz_1\,dz_2\,,\end{aligned} \tag{3.34}$$

[10] Among other things, this means that the figure stands for both sides of the Cutkosky diagram, although only one side is shown — one must bear in mind that the procedure uses matrix elements, i.e. squared amplitudes.

[11] The procedure henceforth is easy to understand, but not necessarily technically rigorous. A more careful approach will be discussed in section 6, which of course will not change the conclusions we shall reach here.

JHEP10(2025)224

which is the two-VBF-side version of eq. (3.32). As it should be clear by construction, $\mathcal{M}^{(m+2)}_{\ell\ell}(p_1,p_2)$ is the matrix element associated with eq. (3.1), $\mathcal{M}^{(m+1)}_{\ell\gamma}(p_1,p_2)$ and $\mathcal{M}^{(m+1)}_{\gamma\ell}(p_1,p_2)$ are the matrix elements associated with

$$\ell^-(p_1)+\gamma(p_2)\longrightarrow\ell^-(k_1)+T\,, \tag{3.35}$$

$$\gamma(p_1)+\ell^+(p_2)\longrightarrow\ell^+(k_2)+T\,, \tag{3.36}$$

respectively, and $\mathcal{M}^{(m)}_{\gamma\gamma}$ is the matrix element associated with

$$\gamma(p_1)+\gamma(p_2)\longrightarrow T\,. \tag{3.37}$$

In all of these matrix elements, the leptons are massless.

In summary, the steps that we have taken are these: starting from a $\ell^+\ell^-\to\ell^+\ell^-+m$-body process with massive leptons which features VBF-like configurations, by means of unitary operations (amounting to adding and subtracting the same quantities), augmented by the resummation of large collinear logarithms due to initial-state branchings of light objects, we have re-expressed its tree-level matrix element in terms of massless-leptons matrix elements of different multiplicities, that are usually associated with LO, δNLO, and δNNLO contributions.

Ultimately, we want to exploit this fact for replacing the LO- and δNLO-like terms with their exact, complete, counterparts, while keeping the δNNLO-like term as a relative $\mathcal{O}(\alpha^2)$ *improvement* of the underlying NLO prediction. Thus, this is not equivalent to performing a complete NNLO calculation and, while technically easier, its work-flow is much less well established than that of the latter; specifically, one needs to be careful to not double count (with either sign) some contributions.

More in detail, we shall arrive at the improved prediction we are seeking by considering the following issues, in turn:

1. Our starting point is eq. (3.34), which shows how to express a massive-lepton matrix element in terms of massless-lepton matrix elements, plus resummation effects — we discuss the physics contents, limitations, and scope of that equation in section 4.

2. One can relate massive- and massless-lepton matrix elements only by introducing some arbitrary quantities (among which, the factorisation scheme, and the way to subtract and/or cutoff singularities) relevant to the latter. We discuss the nature of the massive vs massless description (specifically, the emergence of the mass logarithms by means of the factorisation theorem) in section 5, as well as a tailored cutoff strategy in section 5.1, and the factorisation-scheme dependence of physical predictions in section 5.2.

3. We have simply stated that eq. (3.34) follows from eq. (3.32), essentially by flipping figure 3 w.r.t. an horizontal axis. In section 5.3 we provide the reader with more formal arguments.

4. Finite terms can be exchanged among different contributions to a fixed-order cross section without changing its physical predictions. Such finite terms are typically associated with the remainders of the subtractions of the singularities emerging from the collinear and soft emissions of massless particles. In view of the fact that we shall

JHEP10(2025)224

replace *part of* eq. (3.34) with a complete NLO calculation, it is of crucial importance that the subtractions in the former induce the *same* finite parts as in the latter. Our complete NLO calculation will be based on the FKS formalism; therefore, we shall re-write the δNLO-like parts of eq. (3.34) exactly as in the context of the FKS procedure — this is discussed in section 6.

4 Interpretation

Since the physics contents of eqs. (3.32) and (3.34) are identical, it is easier to start discussing the former, which is less complicated from a technical viewpoint.

The crucial observation is that the kernel $\mathcal{Q}'_{\gamma\ell}$ of eq. (3.31) *coincides* with the kernel relevant to the degenerate $(n+1)$-body contributions in FKS in the case of $\ell \to \gamma\ell$ branchings (see e.g. the formulae in section 4.3 and appendix D of ref. [13]). Likewise, the first term of eq. (3.32) is the $(n+1)$-body contribution to an FKS cross section, for those cases where the soft subtraction is trivial (see section 4.2 of ref. [13]), and when the singularity structure is such that it does not require the use of $\mathcal{S}$ functions (as is the case of eq. (3.2)). This is important, because it shows that the one-leg procedure we have followed here, which deals solely with tree-level matrix elements, is consistent with that relevant to a fully-fledged subtracted NLO computation. However, this does *not* imply that eq. (3.32) exactly coincides with part of the corresponding δNLO result: to mention just the most trivial aspect, for this to happen the first and second terms of eq. (3.32) would need to be further convoluted with $\Gamma_{\ell/\ell}$,[12] while the third term is already in the form that we usually associate with a Born contribution (i.e. an n-body matrix element convoluted with PDFs, per eq. (3.26)). While the convolution with the PDFs is a trivial operation, much more crucially and technically difficult is to make sure that the subtraction in eq. (3.32) exactly (lest one double count) matches the corresponding one of the δNLO computation that will eventually replace it — this point is discussed throughout the following sections, and will finally be addressed in section 6.

We remark that in the context of QED computations, where PDFs have a well defined perturbative expansion, for "Born" to be unambiguously identified one needs some qualifications. In particular, while just above we have used a criterion based on final-state multiplicities (i.e. n- vs $(n+1)$-body, as was done in section 2), we may as well employ a perturbative counting.[13] In doing so, and assuming that Born-level contributions are those of $\mathcal{O}(\alpha^b)$ associated with $\gamma a \to X$, then all terms in eq. (3.32) (on both sides) are of $\mathcal{O}(\alpha^{b+1})$, and this regardless of whether the convolution by $\Gamma_{\ell/\ell}$ is carried out in the first and second terms on the r.h.s. (since $\Gamma_{\ell/\ell} = \mathcal{O}(\alpha^0)$ while $\Gamma_{\gamma/\ell} = \mathcal{O}(\alpha)$).

Two further observations are necessary. Firstly, we point out again that the Z boson plays no role in the manipulations that lead us to eq. (3.32); its effects, including the interference with the photon, are included *exactly* by the matrix element $\mathcal{M}_\ell^{(n+1)}$, whereby $\log Q^2/m_Z^2$ terms are not resummed (as we have argued, this is an operation which is actually not

[12] One must bear in mind that the initial-state parton that comes from the right ($a(p_2)$ in eq. (3.2)) has an idle role in the procedure that leads to eq. (3.32). Therefore, we may or may not (for testing purposes) further convolute with the PDF relevant to that parton, but if we do, we must do so for all of the terms in eq. (3.32).

[13] The two coincide at the tree level and in the absence of PDFs; this is not necessarily true if either of these conditions is relaxed, as is shown by the discussion in the main text.

JHEP10(2025)224

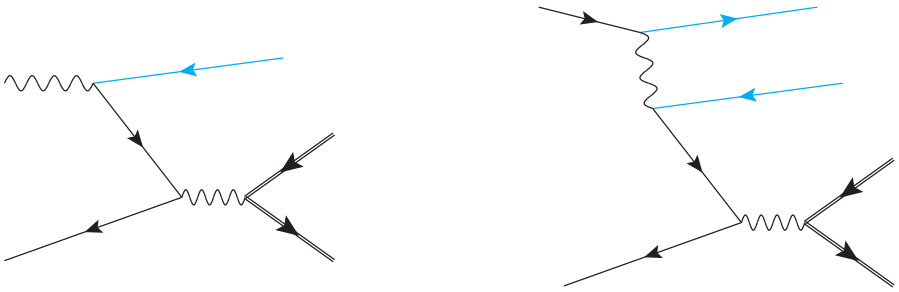

Figure 4. Divergent diagrams that contribute to eq. (3.34); see the text for details.

necessary). Secondly, the role of the second term in eq. (3.32) is that of removing the double counting that stems from the sum of the first and last terms. For this to happen, one needs to bear in mind that the mass-scale squared μ^2 employed in the evaluation of $\mathcal{Q}'_{\gamma\ell}(z)$ must be the same as that used as an argument of the photon PDFs. We also point out that, if one uses the NLL PDFs defined in the Δ scheme [11], by means of a direct computation one finds:

$$\mathcal{Q}'_{\gamma\ell}(z)\Big|_{K_{\gamma\ell}(z)=K^{(\Delta)}_{\gamma\ell}(z)} = \mathcal{Q}_{\gamma\ell}(z)\left[\text{eq. (3.23)}\,,\log\frac{s}{m^2}\longrightarrow\log\frac{s}{\mu^2}\right], \tag{4.1}$$

with $K^{(\Delta)}_{\gamma\ell}(z)$ given in eq. (3.6) of ref. [11]. This is interesting, since as is discussed in section 4.2.3 of ref. [8] the quantity $\mathcal{Q}_{\gamma\ell}(z)$ is one of the possible forms [14] of the Weizsaecker-Williams (WW) function. However, this does *not* mean that in the context of the Δ scheme $\mathcal{Q}'_{\gamma\ell}(z)$ coincides with the WW function because, crucially, of the replacement of the logarithmic term in eq. (4.1): while the WW function is a collinear-divergent quantity, $\mathcal{Q}'_{\gamma\ell}(z)$ is collinear-finite. It remains true that, as far as their forms in the z space are concerned, the two functions are identical, and this is a further evidence of the fact that the Δ scheme is better suited to an intuitive physical picture than the $\overline{\text{MS}}$ one. More extended considerations on this point can be found in section 5.2, section 6.1.2, and in ref. [2].

All of the remarks presented above essentially apply also to eq. (3.34), with some obvious differences. In particular, if one now defines b so that $\mathcal{O}(\alpha^b)$ is relevant to the $\gamma\gamma\to T$ process, then all of the terms in eq. (3.34) are of $\mathcal{O}(\alpha^{b+2})$. In the context of a multiplicity-based counting, the term proportional to $\Gamma_{\gamma/\ell}(z_1)\Gamma_{\gamma/\ell}(z_2)$ is a Born-level one, while all of the others would be part of either an δNLO computation with real processes given by eqs. (3.35) and (3.36) (these are the terms that feature a single $\mathcal{Q}'_{\gamma\ell}(z_{1,2})$ factor or a single $y_{1,2}$ subtraction — of which there are four), or an δNNLO computation with a double-real process given by eq. (3.1) (these are the terms that feature either a factor $\mathcal{Q}'_{\gamma\ell}(z_{1,2})$ or an $y_{1,2}$ subtraction for *each* leg — of which there are four),[14] provided that each of such terms would be convoluted with $\Gamma_{\ell/\ell}$ (which implies one or two convolution(s) for the δNLO- or δNNLO-like terms, respectively).

The key difference w.r.t. what happens with a proper NLO or NNLO computation is that generally the contributions we are considering here are still divergent, since there are no subtractions in some of the singular regions, specifically those which do *not* correspond

[14] An equivalent way of figuring out who is who is to count the number of instances of $\Gamma_{\gamma/\ell}(z_{1,2})$, with zero, one, and two corresponding to δNNLO-like, δNLO-like, and LO contributions, respectively.

JHEP10(2025)224

to VBF-like configurations. Examples of diagrams relevant to the production of $T = \{t, \bar{t}\}$ whose divergences are not subtracted in eq. (3.34) are given in figure 4 — that on the left (an δNLO-type one, associated with an $\mathcal{O}(\alpha)$ $\gamma \to \ell\ell$ splitting kernel) contributes to eq. (3.36), while that on the right (an δNNLO-type one, associated with an $\mathcal{O}(\alpha^2)$ $\ell \to \ell\ell\ell$ splitting kernel) to eq. (3.1).

In both of these examples, the unsubtracted singularities (which can also equivalently be seen as not damped by suitable $\mathcal{S}$ functions) stem from an anti-collinear configuration, here the one in which the outgoing ℓ^+ is collinear to the ℓ^- incoming from the left (the relevant reduced amplitude which is factorised contributes to $\ell^-\ell^+ \to t\bar{t}$ rather than to $\gamma\gamma \to t\bar{t}$ as is the case for VBF-like diagrams). This is clearly a general characteristic in this matter, since anti-collinear configurations cannot be dominant in a VBF-like regime; nevertheless, regardless of their nature and lacking a subtraction they must be avoided, lest eq. (3.34) become meaningless, by means of suitable final-state cuts, to which we shall refer henceforth to as *technical cuts*. Note, finally, that anti-collinear configurations might not be the only sources of unsubtracted divergences; for example, eq. (3.1) receives divergent contributions when $k_1 \,\|\, k_2$, that emerge from a final-state $\gamma \to \ell^+\ell^-$ branching. A more complete discussion on the issues posed by the technical cuts will be given in section 5.1.

In summary, eq. (3.34) will constitute the basis for a relative-$\mathcal{O}(\alpha^2)$ improvement of NLO predictions, the formulation of which requires that one understands the role played by the technical cuts, and finds a precise one-to-one correspondence between some of the terms of eq. (3.34) and those in a proper NLO calculation. On top of that, it is helpful to keep in mind that, prior to any convolution with PDFs, eq. (3.34) is still very strictly related to the $2 \to 2 + m$ massive-lepton matrix element it stems from, which offers some opportunities to test a number of technical issues that emerge in the course of the procedure we shall follow. All of these aspects can be discussed in the context of the factorisation theorem, with which we begin section 5.

5 Technical aspects

As was said before, one key ingredient is the relationship between the massive- and massless-lepton matrix elements, which can be framed in the context of the factorisation theorem.

Before going into that, we preliminarily remind the reader that, while featuring a more complicated divergent structure w.r.t. their massive counterparts, massless-lepton matrix elements have the advantage that, at the tree and one-loop levels, they can be automatically computed and subsequently integrated over the phase space, whereas with a non-zero but small lepton mass the automatic generation of virtual matrix elements is impossible, and the phase-space integration of tree-level ones is difficult. Having said that, if we restrict ourselves to tree-level computations, and assign the lepton a mass which is not too small (roughly speaking, this means using a value of the order of the muon mass), we can still suppose that massive-lepton matrix elements also do not pose major problems from a numerical viewpoint. This implies that, at any fixed order, both its logarithmic and non-logarithmic terms can be obtained numerically, which is sufficient for our needs, since as we have mentioned before we shall employ the massive-lepton matrix elements solely for cross-checking results at the (integrated) matrix-element level.

JHEP10(2025)224

Coming to the factorisation theorem proper, among other things one can exploit it to study analytically the logarithms that appear in the massive-lepton matrix elements. By omitting parton indices in order to simplify the notation, we write it symbolically thus:[15]

$$d\bar{\sigma} = \Gamma \star \Gamma \star d\hat{\sigma} + \mathcal{O}((m^2/Q^2)^c)\,, \tag{5.1}$$

where the $\star$ symbol denotes an x-space convolution, and

$$d\bar{\sigma} = \sum_{i=0}^{\infty} \left(\frac{\alpha}{2\pi}\right)^i d\bar{\sigma}^{[i]}\,, \qquad d\hat{\sigma} = \sum_{i=0}^{\infty} \left(\frac{\alpha}{2\pi}\right)^i d\hat{\sigma}^{[i]}\,, \qquad \Gamma = \sum_{i=0}^{\infty} \left(\frac{\alpha}{2\pi}\right)^i \Gamma^{[i]}\,, \tag{5.2}$$

are the perturbative expansions of the complete massive-lepton cross sections, massless-lepton cross sections, and PDFs, respectively. By replacing eq. (5.2) into eq. (5.1), by expanding the two sides in a series of α, and by equating the emerging terms with the same power of α, one relates the $d\bar{\sigma}^{[i]}$ and $d\hat{\sigma}^{[i]}$ coefficients. The first two orders give (since $\Gamma^{[0]} = \delta(1-z)$ for the lepton, and $\Gamma^{[0]} = 0$ for all of the other partons):

$$d\bar{\sigma}^{[0]} = d\hat{\sigma}^{[0]}\,, \tag{5.3}$$

$$d\bar{\sigma}^{[1]} = d\hat{\sigma}^{[1]} + d\delta^{[1]}\,, \tag{5.4}$$

where

$$d\delta^{[1]} = \Gamma^{[1]} \star \Gamma^{[0]} \star d\hat{\sigma}^{[0]} + \Gamma^{[0]} \star \Gamma^{[1]} \star d\hat{\sigma}^{[0]}\,. \tag{5.5}$$

We stress again that we understand that the two sides of eqs. (5.3) and (5.4) generally differ by power-suppressed terms $(m^2/Q^2)^c$, per eq. (5.1), since these are neglected on the r.h.s.'s. By construction, $d\hat{\sigma}^{[1]}$ is mass-independent and IR-finite, and therefore $d\delta^{[1]}$ accounts for the entire mass-logarithmic behaviour of $d\bar{\sigma}^{[1]}$, which stem from $\Gamma^{[1]}$ — see eq. (3.28), and from its lepton counterpart, eq. (**I**.4.121):

$$\Gamma^{[1]}_{\ell/\ell}(z) = \left[\frac{1+z^2}{1-z}\left(\log\frac{\mu^2}{m^2} - 2\log(1-z) - 1\right)\right]_+ + K_{\ell\ell}(z)\,, \tag{5.6}$$

where the plus distribution implements soft-photon subtractions. We point out that the previous statement holds in an *inclusive* sense — before any integration is carried out, $d\bar{\sigma}^{[1]}$ and $d\delta^{[1]}$ live in an $(n+1)$- and n-body phase space, respectively.[16] In particular, for the logarithmic structure which is explicit in the latter to appear in the former, an integration must be carried out over the extra degrees of freedom present in the $(n+1)$-body phase space w.r.t. those of the n-body one. It is precisely this numerical integration that is problematic in the case of massive-lepton matrix elements. However, if such an integration is successful, the independent calculation of the two sides of eq. (5.4) constitutes a powerful check of the consistency of one's results for the massive- and massless-lepton matrix elements, as well as for the analytical understanding of the mass-logarithmic structure of the former.

[15] The rightmost term in eq. (5.1) reminds one of the existence of power-suppressed effects associated with lepton masses. Since these effects are negligible, henceforth we shall understand them.

[16] It is actually slightly more complicated than this. In the context of an NLO calculation, $d\bar{\sigma}^{[1]}$ features *also* n-body-like contributions (e.g. the soft remainders); however, this does not change the essence of what is said here, which applies to tree-level matrix elements that play the dominant role in the matter we are discussing.

JHEP10(2025)224

The lepton-mass logarithms in eqs. (3.28) and (5.6) are in one-to-one correspondence with subtractions of initial-state collinear singularities, examples of which are given by the plus distributions in eqs. (3.32) and (3.34), in the sense that the angular integrations that give rise to them in the context of a massive-lepton computation correspond to the angular integrations which are subtracted in a massless-lepton computation; in the former, the mass screens the singularities which are subtracted in the latter. One can also consider the screening of any singularity by means of a cut; loosely speaking, if one denotes by y_c the largest value that the angular variable y_i of eqs. (3.32) and (3.34) may assume, (i.e., $-1 \le y_i \le y_c$ rather than $-1 \le y_i \le 1$), then the mass logarithm becomes:

$$\log \frac{\mu^2}{m^2} \quad \longrightarrow -\log\left(\frac{1-y_c}{2}+\frac{m^2}{\mu^2}\right) . \tag{5.7}$$

The r.h.s. of eq. (5.7) with $m \to 0$ shows also what happens if a massless calculation is not collinear-subtracted but cutoff-ed. At $y_c \to 1$ the massive-lepton result displays again the mass logarithm, whereas the (unsubtracted and without cutoff) massless-lepton one diverges. Conversely, if $m^2/\mu^2 \ll 1-y_c$ the two kinds of calculation feature the same logarithmic dependences on the cutoff y_c.

We shall soon show how this is relevant to our case. In order to do that, we extend the procedure above to $\mathcal{O}(\alpha^{b+2})$, whereby the analogue of eqs. (5.3) and (5.4) reads as follows:

$$d\bar{\sigma}^{[2]} = d\hat{\sigma}^{[2]} + d\delta^{[2]} , \tag{5.8}$$

with

$$d\delta^{[2]} = d\delta_D^{[2]} + d\delta_S^{[2]} , \tag{5.9}$$

$$d\delta_D^{[2]} = \left(\Gamma^{[1]} \star \Gamma^{[1]} + \Gamma^{[2]} \star \Gamma^{[0]} + \Gamma^{[0]} \star \Gamma^{[2]}\right) \star d\hat{\sigma}^{[0]} , \tag{5.10}$$

$$d\delta_S^{[2]} = \left(\Gamma^{[1]} \star \Gamma^{[0]} + \Gamma^{[0]} \star \Gamma^{[1]}\right) \star d\hat{\sigma}^{[1]} . \tag{5.11}$$

Equation (5.10) is essentially a doubly-logarithmic contribution, although single logarithms are present there as well. Conversely, eq. (5.11) features only single logarithms; the drawback is that its r.h.s. also depends on the subtracted $\mathcal{O}(\alpha^{b+1})$ coefficient $d\hat{\sigma}^{[1]}$, which may not be readily available in the context of a massive-lepton computation. In order to eliminate it, we can exploit eq. (5.4), to arrive at:

$$d\delta_S^{[2]} = d\delta_{Se}^{[2]} - d\delta_{Sc}^{[2]} , \tag{5.12}$$

with

$$d\delta_{Se}^{[2]} = \left(\Gamma^{[1]} \star \Gamma^{[0]} + \Gamma^{[0]} \star \Gamma^{[1]}\right) \star d\bar{\sigma}^{[1]} , \tag{5.13}$$

$$d\delta_{Sc}^{[2]} = \left(2\,\Gamma^{[1]} \star \Gamma^{[1]} + \left(\Gamma^{[1]} \star \Gamma^{[1]}\right) \star \Gamma^{[0]} + \Gamma^{[0]} \star \left(\Gamma^{[1]} \star \Gamma^{[1]}\right)\right) \star d\hat{\sigma}^{[0]} . \tag{5.14}$$

In eq. (5.13) only unsubtracted massive-lepton matrix elements appear; however, there are now double logarithms, which are cancelled by those in eq. (5.14). It should be clear that while we have understood logarithms of m^2/μ^2, when a cutoff is present we can actually have the more involved argument that appears on the r.h.s. of eq. (5.7),

JHEP10(2025)224

It is appropriate to comment explicitly on the physical meaning of the various contributions that appear in eqs. (5.10), (5.13)(5.14): for example $\Gamma^{[1]} \star \Gamma^{[1]}$ stems from two $1 \to 2$ branchings, one for each incoming leg, while $\Gamma^{[0]} \star \Gamma^{[2]}$ stems from one $1 \to 3$ branching in the leg incoming from the right, and $\Gamma^{[0]} \star (\Gamma^{[1]} \star \Gamma^{[1]})$ is its strongly-ordered analogue, i.e. one that stems from two consecutive $1 \to 2$ branchings from the same right leg. This also renders it clear that only terms such as $\Gamma^{[1]} \star \Gamma^{[1]}$ are possibly associated with VBF configurations; diagrammatically, $\Gamma^{[0]} \star \Gamma^{[2]}$ can be seen to emerge from situations analogous to that depicted on the right panel of figure 4, i.e. from what has been called an anti-collinear configuration.

The latter observation is key in view of the fact that eq. (5.8) can be used in the same way as what was suggested for eq. (5.4), namely as a tool to check the mutual consistency between massive- and massless-lepton matrix element computations. Clearly, some attention is required, since at relative $\mathcal{O}(\alpha^2)$ we restrict ourselves to considering tree-level matrix elements, whereas the quantities $d\bar{\sigma}^{[i]}$ and $d\hat{\sigma}^{[i]}$ are supposed to be the complete cross sections. However, as was already observed, the emergence of mass logarithms is chiefly driven by tree-level matrix elements, and this can indeed be verified explicitly. Thus, for the case of interest for this paper, we shall identify the l.h.s. of eq. (5.8) with the massive-lepton tree-level matrix element of the $2 \to 2 + m$ process, while its r.h.s. will be given by eq. (3.34), with the photon PDFs there ($\Gamma_{\gamma/\ell}$) replaced by their $\mathcal{O}(\alpha)$ coefficients $(\alpha/(2\pi)\Gamma^{[1]}_{\gamma/\ell})$. It should then be clear that this operation does lead to a potential mismatch — specifically, contributions corresponding to terms such as $\Gamma^{[0]} \star \Gamma^{[2]}$ and $\Gamma^{[0]} \star (\Gamma^{[1]} \star \Gamma^{[1]})$ will feature double and single mass logarithms in the massive computation, and logarithms of the cutoff used to impose the technical cuts in the massless computation. There are therefore two things that can be done. One first puts the massive- and massless-lepton results on the same footing, by introducing the same cutoff for the anti-collinear configurations in the two cases, whereby the formal replacement of eq. (5.7) becomes relevant. Then one can either compare the results when $m^2/\mu^2 \ll 1 - y_c$, where an agreement is expected if the procedure that leads to eq. (3.34) is correct. Or one can compare the cutoff-ed massless calculation with the massive one where no cutoff is applied — any significant difference found between the two would signal a possible bias on the predictions of eq. (3.34) due to the cutoff choice. We shall discuss these two options, as well as a number of other issues relevant to the technical cuts, in section 5.1.

5.1 Cuts

As is discussed both in section 4 (see in particular figure 4 there) and at the beginning of section 5, eq. (3.34) requires technical cuts lest it diverge, since its δNLO- and δNNLO-type contributions are not fully-fledged δNLO and δNNLO computations, and thus feature unsubtracted singularities. While the advocated replacement of the δNLO-type terms with a complete δNLO computation will address the former case, for the latter one cuts will still be necessary. By construction, such cuts will be applied on the outgoing leptons. A preliminary question then arises, namely whether and how these cuts will affect not only the contribution on the first line of eq. (3.34), but also the three other ones (where one or both of the outgoing leptons are remnants collinear to the parent beam line, and do not formally appear in the final state). Note that the latter three terms have essentially the same forms, and thus pose the same problems, as the counterevents in the former.

JHEP10(2025)224

As to the "whether", the answer appears to be positive. Physically, this can be argued as follows. All contributions to eq. (3.34) emerge from manipulating the matrix elements of eq. (3.1) by means of kinematical transformations, enforced by identities such as those of eqs. (3.20) and (3.21). Then, if one multiplies the matrix elements from the very beginning by a string of Θ functions that impose the cuts, these kinematical transformations will affect the arguments of such Θ functions (for example, by turning a hard configuration into a collinear one), but will not eliminate them (of course, this does not prevent some of these Θ functions from being null for certain kinematical configurations). In other words, the various contributions to eq. (3.34) are related to each other, in spite of the fact that one is entitled to deal with each of them independently. More formally, these relationships among contributions can be seen as follows. One starts from the distribution identity:

$$\left(\frac{1}{1-y}\right)_+ = \left(\frac{1}{1-y}\right)_{\delta_{\rm I}} + \log\frac{\delta_{\rm I}}{2}\,\delta(1-y)\,, \tag{5.15}$$

with $0 < \delta_{\rm I} \leq 2$, and having defined:

$$\langle\left(\frac{1}{1-y}\right)_{\delta_{\rm I}}, f\rangle = \int_{-1}^{1}\frac{dy}{1-y}\Big[f(y) - f(1)\Theta(y \geq 1-\delta_{\rm I})\Big]. \tag{5.16}$$

By using the massless limits of the formulae given in section 3 one arrives at the usual factorised expression, e.g. for emissions from leg 1:

$$\begin{aligned}&\log\frac{\delta_{\rm I}}{2}\,\delta(1-y_1)\,(1-y_1)\mathcal{M}^{(n+1)}(p_1,p_2)\,d\phi_{n+1}(p_1,p_2) = \\ &\frac{\alpha}{2\pi}\,\log\frac{\delta_{\rm I}}{2}\,P(z_1)\mathcal{M}^{(n)}(z_1p_1,p_2)\,dz_1\,d\phi_n(z_1p_1,p_2)\,,\end{aligned} \tag{5.17}$$

where P is the relevant Altarelli-Parisi kernel. By employing eq. (5.15) to eliminate all of the plus distributions that appear in eq. (3.34), and by subsequently using eq. (5.17) to manipulate all of the emerging terms that feature a $\delta(1-y_{1,2})$ distribution, it is matter of simple algebra to arrive at a result which is identical to that of eq. (3.34), bar for the formal replacements:

$$\left(\frac{1}{1-y_{1,2}}\right)_+ \longrightarrow \left(\frac{1}{1-y_{1,2}}\right)_{\delta_{\rm I}}, \tag{5.18}$$

$$\mathcal{Q}'_{\gamma\ell}(z) \longrightarrow \mathcal{Q}^{(\delta_{\rm I})'}_{\gamma\ell}(z)\,, \tag{5.19}$$

where

$$\mathcal{Q}^{(\delta_{\rm I})'}_{\gamma\ell}(z) = \frac{1+(1-z)^2}{z}\left(\log\frac{s\delta_{\rm I}}{2\mu^2} + 2\log(1-z)\right) + z - K_{\gamma\ell}(z)\,. \tag{5.20}$$

Note that the result of eq. (5.20) coincides with that of section 4.3 of ref. [13], again in keeping with a fact remarked in section 4 — $\mathcal{Q}^{(\delta_{\rm I})'}_{\gamma\ell}$ is the kernel relevant to the FKS degenerate $(n+1)$-body contributions. It now becomes apparent that the various terms of eq. (3.34) are related to each other, since the dependence on $\delta_{\rm I}$ only cancels in their sum, and not in each of them individually.

The procedure above also helps clarify how the technical cuts must be implemented on the second, third, and fourth contributions to eq. (3.34), as well as in the counterevents of

JHEP10(2025)224

the first contribution there, since it underscores how the terms that feature the $\Gamma_{\gamma/\ell}(z_{1,2})$ and $\mathcal{Q}_{\gamma\ell}^{(\delta_I)'}(z_{1,2})$ kernels have emerged from the strictly collinear $\ell \to \gamma\ell$ branching enforced by a $\delta(1-y_{1,2})$ factor; thus, the lepton which does not explicit appear in the final state travels along the beamline with momentum equal[17] to $(1-z_{1,2})p_{1,2}$.

Finally, as far as the technical cuts proper are concerned, and in reference to the process of eq. (3.1) and to the reduced ones emerging from it according to the various contributions to eq. (3.34): the anticollinear divergences are avoided by imposing the following conditions (hemisphere cuts):[18]

$$\Theta_{H_1}\Theta_{H_2} \equiv \Theta\left(\eta_{\ell^-(k_1)} \geq -\eta_c\right)\Theta\left(\eta_{\ell^+(k_2)} \leq \eta_c\right) \tag{5.21}$$

(or equivalent ones given in terms of angles), with $\eta_{\ell(k)}$ the pseudorapidity of lepton ℓ with momentum k, and η_c an arbitrary quantity, understood to be positive. If either (or both) lepton(s) is (are) in the respective anticollinear region, the product in eq. (5.21) vanishes. Conversely, its collinear limits exist, and therefore these cuts are collinear safe. In addition to them, the requirement that the $\gamma \to \ell^+\ell^-$ and $Z \to \ell^+\ell^-$ branchings (the latter when the Z width is set equal to zero) do not induce singularities is equivalent to using

$$\Theta_\gamma = \Theta\left(M_{\ell^-(k_1)\ell^+(k_2)} \geq \delta_{M_1}\right), \tag{5.22}$$

$$\Theta_Z = 1 - \Theta\left(M_Z - \delta_{M_2} \leq M_{\ell^-(k_1)\ell^+(k_2)} \leq M_Z + \delta_{M_3}\right), \tag{5.23}$$

for some δ_{M_1}, δ_{M_2}, and δ_{M_3}; these cuts are manifestly soft and collinear safe. The overall technical cuts amount to imposing

$$\Theta_{H_1}\Theta_{H_2}\Theta_\gamma\Theta_Z\,. \tag{5.24}$$

This implies that the outgoing leptons must be in their respective hemisphere (which includes the case when either of them is a beam remnant). There, they must also pass the invariant mass cuts, that force the pair to not be on the γ and Z mass shells. If either lepton is outside of its hemisphere the event is discarded, and the invariant mass cuts are irrelevant.

We note that there is some redundancy in the cuts of eq. (5.24). For example, in the anticollinear region the contribution due to the graph on the left panel of figure 4 has both[19] $\Theta_{H_2} = 0$ and $\Theta_\gamma = 0$. Still, it seems preferable (owing to its larger flexibility, with only a very minor increase of complexity) to implement both the hemisphere and the invariant-mass cuts in the context of phenomenology studies.

5.2 Factorisation scheme dependence

Lepton PDFs can be computed in perturbative QED only after making some assumptions; these, we collectively call a "scheme". At the LL the choice of a scheme (which is *not* a

[17] This is strictly true only at $\mathcal{O}(\alpha)$, i.e. for $\mathcal{Q}_{\gamma\ell}^{(\delta_I)'}(z_{1,2})$ but not necessarily for $\Gamma_{\gamma/\ell}(z_{1,2})$, which in general contains terms to all orders. By associating all of the remnant momentum with the lepton we make the simplest choice, which is still compatible with the perturbative order we are working at.

[18] In other words: the cutoff parameters in eqs. (5.21), (5.22) and (5.23) play the role in the actual computations of what has been generically denoted by y_c in eq. (5.7).

[19] Note that for this to happen the role of the beam-remnant lepton in defining the cuts is crucial.

JHEP10(2025)224

factorisation scheme, since it is not associated with the subtraction of a singularity) typically involves quantities which are beyond accuracy — see e.g. eqs. (A.14)–(A.19) in ref. [12]. Note that differences among LL schemes may or may not be parametric, and as such can be very large and difficult to quantify; for example, some LL PDFs (notably, those which have been used historically) do not have any photon content, others do. Conversely, at the NLL any scheme *is* a factorisation scheme,[20] that essentially defines the non-divergent part of the subtraction of the collinear singularities of bare PDFs. It is convenient to parametrise factorisation schemes in terms of the $K_{ij}(z)$ functions, given that these also enter the FKS short-distance cross sections (specifically, in the $(n+1)$-body degenerate contributions).

Since we emphasise the importance of accuracy and of the ability to sensibly assess theoretical uncertainties, we discuss here in the main text the case of NLL PDFs; some facts of relevance to their LL counterparts are given in appendix F.

The basic idea is that the factorisation theorem, eq. (5.1), is scheme-independent up to higher-order terms (i.e. those not included in the short-distance cross sections). Thus, in eq. (5.1) the scheme dependence of the PDFs Γ cancels that of the cross sections $d\hat{\sigma}$. At the NLO this is understood in minute details; mnemonically, one bears in mind that the K_{ij} functions enter linearly with a plus sign in the expansions of the PDFs (see e.g. eqs. (3.28) and (5.6)), and with a minus sign in the kernels of the $(n+1)$-body degenerate contributions (see e.g. ref. [13]), so that the physical cross sections (after a perturbative expansion in α) are K_{ij}-independent. At the NNLO the principle is the same, but there are no explicit studies of this matter for leptonic collisions. We point out that the $\mathcal{O}(\alpha^{b+2})$ contributions we are considering here only account for some terms of a proper δNNLO result. However, we can observe that in the combinations

$$\Gamma_{\gamma/\ell}(z) + \frac{\alpha}{2\pi}\,\mathcal{Q}'_{\gamma\ell}(z) \equiv \frac{\alpha}{2\pi}\,\mathcal{Q}_{\gamma\ell}(z) + \mathcal{O}(\alpha^2) \tag{5.25}$$

that appear in eq. (3.34) the dependence on $K_{\gamma\ell}(z)$ drops out at this order after expanding the PDF (see eqs. (3.28) and (3.31)). While this is true by the construction of $\mathcal{Q}'_{\gamma\ell}$, which inherits the $K_{\gamma\ell}$ dependence from $d\hat{\sigma}^{(n)}_{\gamma\mathcal{O}(\alpha)}$, i.e. from the expansion of the photon PDF itself, it will become a useful cross-check tool when the two terms on the l.h.s. of eq. (5.25) will be associated with different contributions to a cross section.

These observations have implications for what has been discussed at the beginning of section 5. Note, in particular, that $d\delta^{[1]}$, $d\delta^{[2]}_D$, and $d\delta^{[2]}_S$ are scheme-dependent through $\Gamma^{[1]}$ and $\Gamma^{[2]}$.[21] Further to this observation, we note that the r.h.s. of eqs. (5.4) and (5.8) are truly scheme independent only if $d\hat{\sigma}^{[1]}$ and $d\hat{\sigma}^{[2]}$, respectively, feature collinear-remainder contributions (the $(n+1)$-degenerate terms of FKS), and not only real-emission ones. This is because the subtractions of collinear singularities of a massless matrix element is inherently defined up to finite terms, whose arbitrariness is compensated by that of the collinear

[20] There is actually a dependence on the renormalisation scheme as well, which is of a different nature w.r.t. that associated with the factorisation scheme. This point has been discussed at length in ref. [12], and will not be repeated here, where we shall always consider the renormalisation scheme as given, choosing the G_μ one for numerical predictions.

[21] The former point renders it clear that when employing the WW function in the definition of the subtraction terms one introduces uncertainties which are difficult to quantify, since there is no known scheme in which the first-order coefficient in the expansion of the photon PDF coincides with the WW function.

JHEP10(2025)224

remainders. In the context of the massive- vs massless-lepton checks that we have discussed in section 5.1 the actual cancellation of all arbitrary terms of collinear origin is automatically taken care of by the presence of the scale- and scheme-independent linear combination on the l.h.s. of eq. (5.25). Explicit results that show the extent of such a cancellation are given in section 6.1.2, and in ref. [2].

5.3 Two-side vs one-side VBF topologies

The main result of this paper will stem from eq. (3.34). In order to arrive from the latter to the improved prediction we seek, we need to investigate a couple of potential issues on top of those that have already been considered. Firstly, how eq. (3.34) emerges by "iterating" the procedure that leads to eq. (3.33). Secondly, the identification of certain terms with δNLO-type contributions (according to the FKS formalism) is based on the fact that the former and the latter have the same *functional* form. However, this does not mean that they are identical. This is because the angular variables $y_{1,2}$ of eq. (3.34) are defined in the rest frame of p_1+p_2, while FKS would require y_1 (y_2) to be defined in the rest frame of $p_1+z_2p_2$ ($z_1p_1+p_2$), since this is the c.m. frame of the parton pair that initiates the hard process. As we shall see in the following, these two items are related to each other to a certain extent; we shall start our discussion from the former.

By "iterating" the procedure that leads to eq. (3.33) we literally mean to apply it separately to the following two quantities:

$$\left(\frac{1}{1-y_1}\right)_+\left((1-y_1)\mathcal{M}_{\ell\ell}^{(m+2)}\right)d\phi_{m+2}(p_1,p_2)\,, \tag{5.26}$$

$$\left(\Gamma_{\gamma/\ell}(z_1)+\frac{\alpha}{2\pi}\,\mathcal{Q}'_{\gamma\ell}(z_1)\right)\mathcal{M}_{\gamma\ell}^{(m+1)}\,d\phi_{m+1}(z_1p_1,p_2)\,dz_1\,. \tag{5.27}$$

It is apparent that the former generates the first and the second contributions in eq. (3.34), and the latter the third and the fourth. However, eq. (3.33) has been obtained by starting from a massive matrix element ($\overline{\mathcal{M}}_{\ell\ell}^{(m+2)}$), and a massive $(m+2)$-body phase space — which is not what appears in eqs. (5.26) and (5.27). The key observation is the factorised structure of the VBF-like contributions we are considering. Such a structure implies that the characteristics of the vertex where the photon branches from $\ell^+(p_2)$ are not affected by the form of the contributions to the matrix elements relevant to the vertex where the photon branches from $\ell^-(p_1)$, which here give rise the y_1- and z_1-dependent prefactors in eqs. (5.26) and (5.27), respectively. Because of this, we can easily restore the mass dependence of the $\ell^+(p_2)\to\gamma\ell^+(k_2)$ vertex in the $\mathcal{M}_{\ell\ell}^{(m+2)}$ and $\mathcal{M}_{\gamma\ell}^{(m+1)}$ matrix elements — this is sufficient to give one the collinear-dominant contributions. Likewise, the phase spaces can again be taken to be massive. In this way, the only remaining difference w.r.t. the original starting point is the presence, in eq. (5.27) of an $(m+1)$-body phase space, rather than of an $(m+2)$-body one. In fact, the implicit assumption is that such a phase space is written as follows:

$$d\phi_{m+1}(z_1p_1,p_2)dz_1=\left(\frac{s\xi_1}{4}\frac{1}{2(2\pi)^2}\right)^{-1}\delta(1-y_1)\,d\phi_{m+2}(p_1,p_2)\,. \tag{5.28}$$

Again, the prefactors on the r.h.s. of this equation do not have any bearings on the features relevant to the second step of the procedure considered here, since the latter are essentially

JHEP10(2025)224

limited to parametrising $p_2\cdot k_2$. By employing eq. (5.28) one also still works in the rest frame of p_1+p_2. In this way, one finally arrives at eq. (3.34), where by construction all of the angular variables are defined in the rest frame of p_1+p_2.

An alternative and more rigorous way to obtain eq. (3.34) is that of observing that the two collinear limits of interest, namely $p_1 \parallel k_1$ and $p_2 \parallel k_2$, are independent of each other — the double-collinear limit is incoherent:

$$\begin{aligned}\overline{\mathcal{M}}_{\ell\ell}^{(n+2)} &\xrightarrow{p_1\parallel k_1} \frac{e^2}{p_1\cdot k_1 - m^2}\, P^{<}_{\gamma^\star\ell}(z_1)\, \mathcal{M}_{\gamma}^{(n+1)}(zp_1,p_2) \\ &\xrightarrow{p_2\parallel k_2} \frac{e^2}{p_1\cdot k_1 - m^2}\, P^{<}_{\gamma^\star\ell}(z_1)\, \frac{e^2}{p_2\cdot k_2 - m^2}\, P^{<}_{\gamma^\star\ell}(z_2)\, \mathcal{M}_{\gamma\gamma}^{(n)}(z_1p_1,z_2p_2)\,.\end{aligned} \tag{5.29}$$

Thus, the identities of eqs. (3.20) and (3.21), written in terms of

$$\rho_1 = 2\frac{(1-\xi_1)^2}{\xi_1^2}\frac{m^2}{s}\,, \qquad \rho_2 = 2\frac{(1-\xi_2)^2}{\xi_2^2}\frac{m^2}{s}\,, \tag{5.30}$$

can be exploited simultaneously for the two incoming legs, as a factorised series expansion in (ρ_1,ρ_2).

What was done above, and in particular eq. (5.28), allows us to discuss the second of the items introduced at the beginning of this section. Here, we can formulate it as follows: while eq. (5.28) gives one a way to obtain the sought result, it is by no means *necessary* to use it. Then, what happens if one tries and works in the rest frame of $z_1p_1+p_2$? This is an equally valid approach, since the massification of the matrix elements and of the phase space is as before.

In order to follow the details of this discussion, the reader will need some information about the reference frames relevant to the problem, and to exploit an identity among distributions, which is proven in appendix E. As far as the former ones are concerned, we present all of the material about them in appendix D; here, we limit ourselves to introduce the notation with which we identify the frames that we shall employ in the following, namely:

$$F: \quad \text{rest frame of } p_1+p_2\,, \tag{5.31}$$

$$F_1': \quad \text{rest frame of } z_1p_1+p_2\,. \tag{5.32}$$

With the help of appendix D and of appendix E, we are now able to consider the iteration of our procedure starting from the quantity in eq. (5.27) but, at variance with what has been done before, we shall not employ eq. (5.28) but work directly in frame F_1'. By using the notation of eqs. (3.12) and (3.13) this leads to:

$$\begin{aligned}&\left(\Gamma_{\gamma/\ell}(z_1) + \frac{\alpha}{2\pi}\,\mathcal{Q}'_{\gamma\ell}(z_1;s)\right)\left(\frac{1}{1-\bar{y}_2}\right)_+\Big((1-\bar{y}_2)\mathcal{M}_{\gamma\ell}^{(m+1)}(z_1p_1,p_2)\Big) \\ &\times d\tilde{\phi}_n(p_1,p_2)\frac{1}{2(2\pi)^3}\,\frac{z_1 s}{4}\,\bar{\xi}_2 d\bar{\xi}_2\, d\bar{y}_2\, d\varphi_2\, dz_1 \\ &+\left(\Gamma_{\gamma/\ell}(z_1) + \frac{\alpha}{2\pi}\,\mathcal{Q}'_{\gamma\ell}(z_1;s)\right)\left(\Gamma_{\gamma/\ell}(z_2) + \frac{\alpha}{2\pi}\,\mathcal{Q}'_{\gamma\ell}(z_2;z_1 s)\right) \\ &\times \mathcal{M}_{\gamma\gamma}^{(m)}(z_1p_1,z_2p_2)\, d\phi_m(z_1p_1,z_2p_2)\, dz_1\, dz_2\,,\end{aligned} \tag{5.33}$$

JHEP10(2025)224

which must be compared to the last two lines of eq. (3.34). There are two obvious differences emerging from such a comparison, namely: the plus prescription is expressed in terms of the $\bar{y}_2$ variable (as opposed to y_2), which is due to working in frame F_1' rather than in F; as a consequence of this, the integration variables are also those relevant to the former frame. And secondly, the rightmost $\mathcal{Q}'_{\gamma\ell}$ term in the last line of eq. (5.33) features a $(z_1 s)$ factor as argument of the logarithm that multiplies the Altarelli-Parisi splitting kernel, rather than s; in view of this, the notation has been modified. In order to proceed, in the first term of eq. (5.33) one uses eq. (E.11) and changes variables[22] $(\bar{y}_2, \bar{\xi}_2) \to (y_2, \xi_2)$; furthermore, one also observes that:

$$1 - \bar{y}_2 = \frac{4}{z_1 s \bar{\xi}_2} (p_2 \cdot k_2) = \frac{\xi_2}{z_1 \bar{\xi}_2} (1 - y_2). \tag{5.34}$$

After some algebra, the first term of eq. (5.33) thus transformed results in the sum of two contributions, the first of which is identical to the third line of eq. (3.34), while the second of which reads:

$$\begin{aligned} &\left(\Gamma_{\gamma/\ell}(z_1) + \frac{\alpha}{2\pi} \mathcal{Q}'_{\gamma\ell}(z_1; s)\right) \left(-\frac{\alpha}{2\pi} \log z_1 \, P_{\gamma\ell}(z_2)\right) \\ &\times \mathcal{M}^{(m)}_{\gamma\gamma}(z_1 p_1, z_2 p_2) \, d\phi_m(z_1 p_1, z_2 p_2) \, dz_1 \, dz_2 \,, \end{aligned} \tag{5.35}$$

where use has been made of eq. (5.17) to simplify the purely collinear term[23] stemming from $\delta(1 - y_2)$. Then, in the sum of eq. (5.35) plus the second term of eq. (5.33) one finds the linear combination:

$$- \log z_1 P_{\gamma\ell}(z_2) + \mathcal{Q}'_{\gamma\ell}(z_2; z_1 s) \equiv \mathcal{Q}'_{\gamma\ell}(z_2; s). \tag{5.36}$$

This is identical to what appears in the last line of eq. (3.34), thus finally proving that, regardless of whether the second step of the iterative procedure is carried out in F or F_1', the result is always the same. We point out that this also shows that the final result is independent of whether one starts with the $p_1 \parallel k_1$ or the $p_2 \parallel k_2$ collinear configuration.

6 The NNLO-improved NLO predictions

We are finally in the position to firmly establish the connection between the various terms in eq. (3.34) and their counterparts in NNLO, NLO, and LO cross sections, and thus to achieve our stated goal of replacing some of the former with some of the latter. We start by re-writing eq. (3.34) as follows (see page 7 for the notation used here):

$$\overline{\mathcal{M}}^{(m+2)}_{\ell\ell} d\phi_{m+2} \longrightarrow d\hat{\Sigma}_{\delta\text{NNLO}_\Gamma} + d\hat{\Sigma}_{\delta\text{NLO}_\Gamma} + d\Sigma_{\text{LO}_\Gamma} \,, \tag{6.1}$$

[22] Note that part of the jacobian of this transformation is already included in eq. (E.11), and thus one need only take into account $d\bar{\xi}_2/d\xi_2$; this, thanks to the fact that $\bar{y}_2$ is independent of ξ_2, and thus the jacobian is the product of two terms.

[23] Note that at $y_2 = 1$ we have $\xi_2 = \bar{\xi}_2$, and therefore there is no need to introduce a variable $\bar{z}_2$.

JHEP10(2025)224

where:

$$
\begin{aligned}
d\hat{\Sigma}_{\delta\text{NNLO}_\Gamma}(p_1,p_2) = &\left(\frac{1}{1-y_1}\right)_+\left(\frac{1}{1-y_2}\right)_+\left((1-y_1)(1-y_2)\mathcal{M}_{\ell\ell}^{(m+2)}\right)d\phi_{m+2}(p_1,p_2)\\
&+\frac{\alpha}{2\pi}\,\mathcal{Q}'_{\gamma\ell}(z_2)\left(\frac{1}{1-y_1}\right)_+\left((1-y_1)\mathcal{M}_{\ell\gamma}^{(m+1)}\right)d\phi_{m+1}(p_1,z_2p_2)\,dz_2\\
&+\frac{\alpha}{2\pi}\,\mathcal{Q}'_{\gamma\ell}(z_1)\left(\frac{1}{1-y_2}\right)_+\left((1-y_2)\mathcal{M}_{\gamma\ell}^{(m+1)}\right)d\phi_{m+1}(z_1p_1,p_2)\,dz_1\\
&+\left(\frac{\alpha}{2\pi}\right)^2\mathcal{Q}'_{\gamma\ell}(z_1)\,\mathcal{Q}'_{\gamma\ell}(z_2)\mathcal{M}_{\gamma\gamma}^{(m)}\,d\phi_m(z_1p_1,z_2p_2)\,dz_1\,dz_2\,,
\end{aligned}
\tag{6.2}
$$

$$
\begin{aligned}
d\hat{\Sigma}_{\delta\text{NLO}_\Gamma}(p_1,p_2) = &\,\Gamma_{\gamma/\ell}(z_2)\left(\frac{1}{1-y_1}\right)_+\left((1-y_1)\mathcal{M}_{\ell\gamma}^{(m+1)}\right)d\phi_{m+1}(p_1,z_2p_2)\,dz_2\\
&+\Gamma_{\gamma/\ell}(z_1)\left(\frac{1}{1-y_2}\right)_+\left((1-y_2)\mathcal{M}_{\gamma\ell}^{(m+1)}\right)d\phi_{m+1}(z_1p_1,p_2)\,dz_1\\
&+\frac{\alpha}{2\pi}\Big(\mathcal{Q}'_{\gamma\ell}(z_1)\Gamma_{\gamma/\ell}(z_2)+\Gamma_{\gamma/\ell}(z_1)\mathcal{Q}'_{\gamma\ell}(z_2)\Big)\\
&\times\mathcal{M}_{\gamma\gamma}^{(m)}\,d\phi_m(z_1p_1,z_2p_2)\,dz_1\,dz_2\,,
\end{aligned}
\tag{6.3}
$$

$$
d\Sigma_{\text{LO}_\Gamma}(p_1,p_2) = \Gamma_{\gamma/\ell}(z_1)\Gamma_{\gamma/\ell}(z_2)\mathcal{M}_{\gamma\gamma}^{(m)}\,d\phi_m(z_1p_1,z_2p_2)\,dz_1\,dz_2\,,
\tag{6.4}
$$

are, as the notation suggests, the δNNLO-, δNLO-, and LO-like contributions, respectively, due to $\gamma\gamma$ fusion. These three quantities are independent of one another,[24] and will be thus manipulated independently. Starting with eq. (6.2), by exploiting eq. (5.15) one arrives at:

$$
\begin{aligned}
d\hat{\Sigma}_{\delta\text{NNLO}_\Gamma}(p_1,p_2) = &\left(\frac{1}{1-y_1}\right)_{\delta_\text{I}}\left(\frac{1}{1-y_2}\right)_{\delta_\text{I}}\left((1-y_1)(1-y_2)\mathcal{M}_{\ell\ell}^{(m+2)}\right)d\phi_{m+2}(p_1,p_2)\\
&+\frac{\alpha}{2\pi}\,\mathcal{Q}_{\gamma\ell}^{(\delta_\text{I})\prime}(z_2)\left(\frac{1}{1-y_1}\right)_{\delta_\text{I}}\left((1-y_1)\mathcal{M}_{\ell\gamma}^{(m+1)}\right)d\phi_{m+1}(p_1,z_2p_2)\,dz_2\\
&+\frac{\alpha}{2\pi}\,\mathcal{Q}_{\gamma\ell}^{(\delta_\text{I})\prime}(z_1)\left(\frac{1}{1-y_2}\right)_{\delta_\text{I}}\left((1-y_2)\mathcal{M}_{\gamma\ell}^{(m+1)}\right)d\phi_{m+1}(z_1p_1,p_2)\,dz_1\\
&+\left(\frac{\alpha}{2\pi}\right)^2\mathcal{Q}_{\gamma\ell}^{(\delta_\text{I})\prime}(z_1)\,\mathcal{Q}_{\gamma\ell}^{(\delta_\text{I})\prime}(z_2)\mathcal{M}_{\gamma\gamma}^{(m)}\,d\phi_m(z_1p_1,z_2p_2)\,dz_1\,dz_2\,.
\end{aligned}
\tag{6.5}
$$

By construction, this short-distance cross section is independent of the arbitrary parameter δ_I. It can be used to define the relative $\mathcal{O}(\alpha^2)$ improvement we have been seeking, thus:

$$
\Delta d\hat{\sigma}_{\delta\text{NNLO}_\Gamma}(p_1,p_2) = d\zeta_1\,d\zeta_2\,\Gamma_{\ell/\ell}(\zeta_1)\,\Gamma_{\ell/\ell}(\zeta_2)\,d\hat{\Sigma}_{\delta\text{NNLO}_\Gamma}(\zeta_1p_1,\zeta_2p_2)\,,
\tag{6.6}
$$

where we have convoluted the short-distance cross section of eq. (6.5) with the lepton PDFs relevant to each incoming leg. We remind the reader that the matrix elements that appear in the four lines of eq. (6.5) are the complete ones (i.e. they are not limited to the contributions of the graphs that feature t-channel vector-boson exchanges) relevant to the processes of eqs. (3.1), (3.35), (3.36), and (3.37), respectively.

[24] In the sense that they are separately IR-finite. One can still exchange finite terms among them, which is what has been anticipated at page 13 and the reason why the various identifications have to be done with utmost care. We shall return to this point later.

JHEP10(2025)224

Equations (6.5) and (6.6) constitute a physical result as long as the two rightmost terms in eq. (6.1) can be identified with the relevant contributions to an NLO and a LO cross section, respectively. This is now easy to do. Specifically, as far as eq. (6.3) is concerned, one starts by rewriting it in the natural frames (according to the FKS subtraction formalism) suggested by the arguments of the various phase spaces. By employing again the results of appendix D and of appendix E (that is, ultimately by performing an operation which is the inverse of that of section 5.3), and the identity of eq. (5.15) we obtain:

$$\begin{aligned} d\hat{\Sigma}_{\delta\text{NLO}_\Gamma}(p_1,p_2) = {}& \Gamma_{\gamma/\ell}(z_2)\left(\frac{1}{1-\bar{y}_1}\right)_{\bar{\delta}_\text{I}}\left((1-\bar{y}_1)\mathcal{M}_{\ell\gamma}^{(m+1)}\right) d\phi_{m+1}(p_1,z_2p_2)\,dz_2 \\ & + \Gamma_{\gamma/\ell}(z_1)\left(\frac{1}{1-\bar{y}_2}\right)_{\bar{\delta}_\text{I}}\left((1-\bar{y}_2)\mathcal{M}_{\gamma\ell}^{(m+1)}\right) d\phi_{m+1}(z_1p_1,p_2)\,dz_1 \\ & + \frac{\alpha}{2\pi}\left(\mathcal{Q}_{\gamma\ell}^{(\bar{\delta}_\text{I})'}(z_1;z_2s)\Gamma_{\gamma/\ell}(z_2) + \Gamma_{\gamma/\ell}(z_1)\mathcal{Q}_{\gamma\ell}^{(\bar{\delta}_\text{I})'}(z_2;z_1s)\right) \\ & \times \mathcal{M}_{\gamma\gamma}^{(m)}\,d\phi_m(z_1p_1,z_2p_2)\,dz_1\,dz_2 \end{aligned} \tag{6.7}$$

$$\equiv d\zeta_1\,\Gamma_{\gamma/\ell}(\zeta_1)\,d\hat{\Sigma}^{(1)}_{\delta\text{NLO}_\Gamma}(\zeta_1p_1,p_2) + d\zeta_2\,\Gamma_{\gamma/\ell}(\zeta_2)\,d\hat{\Sigma}^{(2)}_{\delta\text{NLO}_\Gamma}(p_1,\zeta_2p_2)\,, \tag{6.8}$$

where in the rightmost side we have introduced:[25]

$$\begin{aligned} d\hat{\Sigma}^{(1)}_{\delta\text{NLO}_\Gamma}(p_1,p_2) = {}& \left(\frac{1}{1-\bar{y}_2}\right)_{\bar{\delta}_\text{I}}\left((1-\bar{y}_2)\mathcal{M}_{\gamma\ell}^{(m+1)}\right) d\phi_{m+1}(p_1,p_2) \\ & + \frac{\alpha}{2\pi}\mathcal{Q}_{\gamma\ell}^{(\bar{\delta}_\text{I})'}(z_2;s)\,\mathcal{M}_{\gamma\gamma}^{(m)}\,d\phi_m(p_1,z_2p_2)\,dz_2\,, \end{aligned} \tag{6.9}$$

$$\begin{aligned} d\hat{\Sigma}^{(2)}_{\delta\text{NLO}_\Gamma}(p_1,p_2) = {}& \left(\frac{1}{1-\bar{y}_1}\right)_{\bar{\delta}_\text{I}}\left((1-\bar{y}_1)\mathcal{M}_{\ell\gamma}^{(m+1)}\right) d\phi_{m+1}(p_1,p_2) \\ & + \frac{\alpha}{2\pi}\mathcal{Q}_{\gamma\ell}^{(\bar{\delta}_\text{I})'}(z_1;s)\mathcal{M}_{\gamma\gamma}^{(m)}\,d\phi_m(z_1p_1,p_2)\,dz_1\,, \end{aligned} \tag{6.10}$$

and have renamed $z_1 \to \zeta_1$ ($z_2 \to \zeta_2$) in the second and forth (first and third) terms on the r.h.s. of eq. (6.7), while including such terms in eqs. (6.9) and (6.10), respectively. The two quantities in eqs. (6.9) and (6.10) are separately independent of the arbitrary parameter $\bar{\delta}_\text{I}$; note the augmented dependence of $\mathcal{Q}'_{\gamma\ell}$, which is due to the same mechanism as that which leads to eq. (5.36). This fact, the functional forms, the variables used, render it now easy to see that the two terms of the following expression:

$$\begin{aligned} & d\zeta_1 d\zeta_2\,\Gamma_{\ell/\ell}(\zeta_1)\,\Gamma_{\gamma/\ell}(\zeta_2)\,d\hat{\Sigma}^{(2)}_{\delta\text{NLO}_\Gamma}(\zeta_1p_1,\zeta_2p_2) \\ + {}& d\zeta_1 d\zeta_2\,\Gamma_{\gamma/\ell}(\zeta_1)\,\Gamma_{\ell/\ell}(\zeta_2)\,d\hat{\Sigma}^{(1)}_{\delta\text{NLO}_\Gamma}(\zeta_1p_1,\zeta_2p_2) \end{aligned} \tag{6.11}$$

coincide with the FKS δNLO real-correction contributions for the processes whose tree-level graphs are associated with eqs. (3.35) and (3.36), respectively.

Finally, it is self-evident that eq. (6.4) is already in the form of the LO cross section for the process of eq. (3.37). Therefore, we have established that the decomposition of eq. (6.1)

[25] We point out that we always define $s = (p_1+p_2)^2$, with p_1 and p_2 the arguments of the function we are considering. Ultimately, we want s to be the partonic c.m. energy, i.e. the quantity to be rescaled by the product of the appropriate Bjorken x's, ζ_i.

JHEP10(2025)224

gives rise to a genuine (i.e. that does not double count) δNNLO contribution ultimately in the form of eq. (6.6), which can therefore be safely summed to a complete NLO-accurate cross section. We write this as follows, by employing the notation of eq. (3.26):

$$d\sigma(p_1,p_2) = \sum_{ij} \Gamma_{i/\ell}(\zeta_1)\,\Gamma_{j/\ell}(\zeta_1)\left(d\hat{\sigma}^{[0]}_{ij}(\zeta_1 p_1,\zeta_2 p_2) + \frac{\alpha}{2\pi}\,d\hat{\sigma}^{[1]}_{ij}(\zeta_1 p_1,\zeta_2 p_2)\right) d\zeta_1\,d\zeta_2 + \Delta d\hat{\sigma}_{\delta\text{NNLO}_\Gamma}(p_1,p_2)\,. \tag{6.12}$$

Note that the sums in the first line of eq. (6.12) extend to all parton types, and are not restricted to leptons of the same flavours as the incoming ones. This is in keeping with what the factorisation theorem dictates, and shows explicitly how eq. (6.12) is valid everywhere in the phase space, where it is at least NLO-accurate, with the accuracy increasing effectively to NNLO in the $\gamma\gamma$-dominated regions, thanks to the rightmost term on the r.h.s. In fact, eq. (6.12) can be re-written in a form where its being *the* factorisation-theorem formula, albeit featuring only a subset of the NNLO contributions, is more manifest. This can be done by observing that the matrix elements which appear in eq. (6.5) are such that:

$$\mathcal{M}^{(m+q)}_{ab} \;\propto\; \alpha^b\alpha^q\,, \qquad q=0,1,2\,. \tag{6.13}$$

By also taking into account the explicit α-dependent prefactors in eq. (6.5), eq. (6.13) motivates the definition of the NNLO analogue of the LO and NLO short distance cross sections which appear in the first line of eq. (6.12), thus:

$$\left(\frac{\alpha}{2\pi}\right)^2 d\hat{\sigma}^{[2]}_{\delta\text{NNLO}_\Gamma}(p_1,p_2) = d\hat{\Sigma}_{\delta\text{NNLO}_\Gamma}(p_1,p_2)\,, \tag{6.14}$$

which leads us to:

$$d\sigma(p_1,p_2) = d\zeta_1\,d\zeta_2 \sum_{ij}\Gamma_{i/\ell}(\zeta_1)\,\Gamma_{j/\ell}(\zeta_1) \times\left(d\hat{\sigma}^{[0]}_{ij}(\zeta_1 p_1,\zeta_2 p_2)+\frac{\alpha}{2\pi}\,d\hat{\sigma}^{[1]}_{ij}(\zeta_1 p_1,\zeta_2 p_2)+\delta_{i\ell}\delta_{j\ell}\left(\frac{\alpha}{2\pi}\right)^2 d\hat{\sigma}^{[2]}_{\delta\text{NNLO}_\Gamma}(\zeta_1 p_1,\zeta_2 p_2)\right), \tag{6.15}$$

which is the highly symmetric expression we were seeking.

We conclude by returning to the comment made in footnote 24. By introducing the quantities which appear on the r.h.s. of eq. (6.1), and by treating them independently from one another (in particular as far as the integration over the phase space is concerned), the *local* cancellations between the two terms on the l.h.s. of eq. (5.25) does not occur any longer. Such cancellations are relevant to two quantities: the hard scale μ, and the change-of-scheme function $K_{\gamma\ell}$. Rather than being a problem, this is actually an opportunity to check that the sum of the terms on the r.h.s. of eq. (6.15) is more stable w.r.t. changes of scales and scheme than its individual summands. Note, in particular, that in the context of a strict NLO-accurate computation (e.g. one where only the first two terms within the round brackets on the r.h.s. of eq. (6.15) are retained) the scheme dependence of $\gamma\gamma$-channel contributions is beyond accuracy, being of relative $\mathcal{O}(\alpha^2)$ (each $K_{\gamma\ell}$ function is multiplied by an α factor, and there are no

JHEP10(2025)224

$\mathcal{O}(\alpha^0)$ contributions to the photon PDF). We have shown that such scheme-dependent terms are exactly cancelled, at least in the $\gamma\gamma$-dominated regions, by the cross section in the second line of eq. (6.12). We shall give an actual numerical evidence of this fact in section 6.1.2.

6.1 Results

In this section we present a few sample results which document the impact of the technical cuts (section 6.1.1) and of the choice of factorisation scheme (section 6.1.2) on actual observables.

The δNNLO$_\Gamma$ cross section of eq. (6.5) and (where relevant) the δNLO$_\Gamma$ one of eq. (6.11) have been implemented in a non-automated manner in a dedicated code (some details of which are given in appendices B and C) for the two processes we have considered in this paper, namely $t\bar{t}$ and W^+W^- production. Aside from this implementation, the LO and NLO cross sections are automatically obtained by employing `MadGraph5_aMC@NLO` [15], and specifically its EW-corrections capabilities [12, 16].[26] The basic parameters used for our simulations are as follows:

$$m_W = 80.419 \text{ GeV}\,, \tag{6.16}$$

$$m_Z = 91.188 \text{ GeV}\,, \tag{6.17}$$

$$m_t = 173.3 \text{ GeV}\,, \tag{6.18}$$

$$m_H = 125 \text{ GeV}\,. \tag{6.19}$$

All widths are set equal to zero. Beyond-LO results are obtained in the context of the G_μ renormalisation scheme [17], with

$$G_f = 1.16639{\cdot}10^{-5} \text{ GeV}^{-2} \quad \Longrightarrow \quad \alpha = 1/132.5070\,. \tag{6.20}$$

The hard scale is generally set equal to the pair invariant mass of the massive system produced (i.e. either $t\bar{t}$ or W^+W^-), with additional non-dynamical choices employed in section 6.1.1. We consider $\mu^+\mu^-$ collisions, with the muon NLL PDFs taken from refs. [6, 7].

6.1.1 Impact of the technical cuts

The results concerning the impact of the technical cuts on observables which we present in this section are in keeping with what has been discussed at the end of section 5 and in section 5.1. We have considered $t\bar{t}$ and W^+W^- production in $\mu^+\mu^-$ collisions at different collider energies $\sqrt{S}$. Lest there should be a proliferation of plots, and given that the conclusions we shall reach are essentially process-independent, we show here the results for $t\bar{t}$ production at $\sqrt{S} = 3\,\text{TeV}$ and $10\,\text{TeV}$, while those relevant to W^+W^- production are collected in appendix A. In both cases, we have chosen the pair invariant mass and the transverse momentum of the positively-charged outgoing heavy particle as representative observables; as is the case for the production process, the conclusions would not change if other observables (such as pair and single-inclusive rapidity and pseudorapidity, or pair transverse momentum, all of which we have studied) were shown.

[26] We remind the reader that while the first automation of EW corrections in `MadGraph5_aMC@NLO` had been presented in ref. [16], it did not apply to lepton collisions, but only to hadron ones. The relevant extension has been achieved in ref. [12].

JHEP10(2025)224

The essence of the idea discussed in section 5 which we shall employ here is that of a direct comparison between massive- and massless-lepton predictions. The strictest version of such a comparison at the level of $2 \to 2 + m$ tree-level matrix elements is the one that uses eq. (3.34), with its l.h.s. as is (this is the massive-lepton calculation), and its r.h.s. with the photon PDFs replaced by their $\mathcal{O}(\alpha)$ coefficients $(\alpha/(2\pi)\Gamma^{[1]}_{\gamma/\ell})$, and no convolution with muon PDFs[27] (this is the massless-lepton computation; as its massive counterpart, it is then exactly of $\mathcal{O}(\alpha^{2+m})$). In other words, the latter is NNLO$_\Gamma$ with the PDFs replaced by their $\mathcal{O}(\alpha)$ coefficients; with abuse of notation, we still denote it by NNLO$_\Gamma$. Conversely, the results of the former are denoted by MG, having been obtained by means of an `MadGraph5_aMC@NLO` branch which allows one to keep the light-lepton masses different from zero. In the text, these two simulations will be loosely referred to as "massive" and "massless".

The technical cuts have been applied in the same manner to the massive and massless predictions, with the outgoing leptons dealt with as was explained in section 5.1. We have considered several combinations of cuts. As far as the lepton-pair invariant mass is concerned, and in order to magnify any possible cut dependence, we have chosen (see eqs. (5.22) and (5.23)):

$$\delta_{M_1} = 120 \quad \text{or} \quad 200 \text{ GeV}\,, \tag{6.21}$$

$$\delta_{M_2} = \delta_{M_3} = 0\,. \tag{6.22}$$

As hemisphere cuts, we have considered (see eq. (5.21))

$$\eta_c = 2.5 \quad \text{or} \quad 5\,, \tag{6.23}$$

as well as the rather draconian choice of eliminating at the level of amplitudes the s-channel resonant diagrams, i.e. those in which either the γ or the Z splits into a $\mu^+\mu^-$ pair. In this way, we have obtained six different cut combinations, the bottom line of which is that the hemisphere cuts have a negligible effect when these invariant-mass cuts are also applied (in other words, the latter also act very effectively on anti-collinear configurations). Because of this, we shall only show (as representatives of worst-case scenarios) the predictions obtained with the two invariant mass cuts and no hemisphere cuts, and with the loosest hemisphere cuts ($\eta_c = 5$), and the removal of the s-channel resonant diagrams,[28] calling them as follows:

$$\text{scenario 1}: \quad m(\mu^+\mu^-) \geq 120 \text{ GeV}\,, \tag{6.24}$$

$$\text{scenario 2}: \quad m(\mu^+\mu^-) \geq 200 \text{ GeV}\,, \tag{6.25}$$

$$\text{scenario 3}: \quad \eta_c = 5\,, \quad \text{resonance removal}\,. \tag{6.26}$$

In order to be clear: we do not necessarily advocate such a diagram removal (nor, to a lesser extent, invariant mass cuts without hemisphere cuts) as a solution to be adopted when

[27] We point out that this is equivalent to convoluting with the first-order term of the perturbative expansion of the muon PDF, i.e. with $\delta(1-z)$. This is in keeping with the strict fixed-order comparison strategy we are following here.

[28] For many processes, including but not limited to those studied in this paper, such a removal can be achieved in a gauge-invariant way by considering the production of the relevant final state as initiated by a fictitious $\mu^\pm e^\mp$ pair, with the electron mass set equal to the muon mass.

JHEP10(2025)224

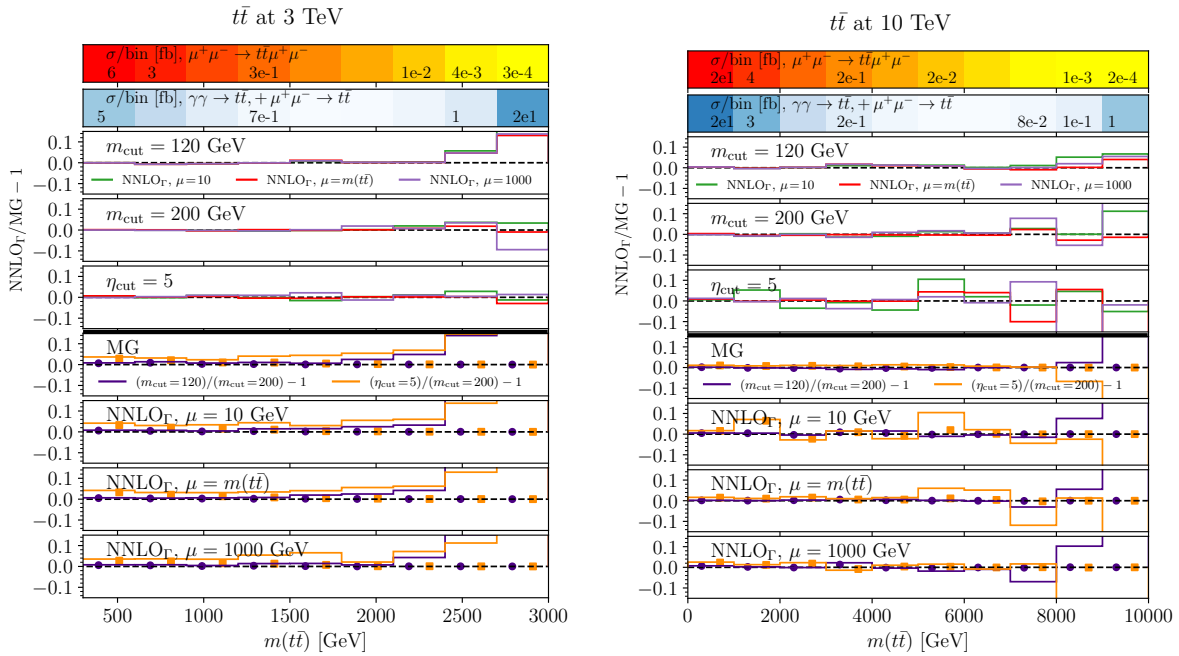

Figure 5. Impact of technical cuts on the $t\bar{t}$ invariant mass, at $\sqrt{S} = 3$ TeV (left panel) and 10 TeV (right panel). The labels are symbolic for eqs. (5.21)–(5.24) and (6.24)–(6.26). See the text for details. Statistical uncertainties are too small to be shown; they are approximately of the same size as the width of the box and circle symbols.

computing cross sections of phenomenological interest. Here, we use it precisely because we are not concerned about phenomenology but rather by the theoretical viability of the strategy proposed in this work, which we are trying to break by means of extreme setups. In keeping with this principle, for each cut scenario we have considered the following three hard-scale choices for the massless calculation:

$$\mu = 10 \text{ GeV}; \qquad \mu = 1000 \text{ GeV}; \qquad \mu = m(t\bar{t}) \quad \text{or} \quad m(W^+W^-)\,. \tag{6.27}$$

Among these, the only one of phenomenological relevance is the third, while the first one is clearly an outlier at a multi-TeV collider.

We now turn to discussing the results we have obtained; as was said above, we shall comment here on $t\bar{t}$ production (figures 5 and 6 for the pair invariant mass and the single-inclusive p_T, respectively), with additional plots relevant to W^+W^- production presented in appendix A (figures 8 and 9). Irrespective of the production process and of the observable, all of the figures have the same layout. At the very top there are two bands, which give one a rough indication of the differential rates, in fb per bin, predicted by: *a)* the massive $2 \to 4$ computation[29] (upper band), and: *b)* the Born-level simulation of $t\bar{t}$ production stemming from the sum of the $\gamma\gamma$ and $\mu^+\mu^-$ channels (lower band). In both bands, darker (lighter) hues correspond to larger (smaller) cross sections; the upper band uses red tones, the lower one blue tones, so that the same cross section in absolute value is associated with two different colours in the two bands. The actual value of the cross section is superimposed to the bands for a few selected bins.

[29] In turn essentially identical, as we shall see, to the massless one emerging from of eq. (3.34) modified as was explained above.

JHEP10(2025)224

The main frame of the figures is composed of two parts, separated by a thick black line, both of which display ratios of cross sections. In the upper part of the main frame there are three ratio plots, with the ratios obtained by dividing a massless prediction by the corresponding massive one, and by subtracting one from the result thus obtained (therefore, an horizontal line at zero would mean perfect agreement between the two predictions). These three ratio plots are obtained with the technical-cut scenarios of eqs. (6.24), (6.25), and (6.26) for the upper, middle, and lower plot, respectively. Each plot shows three histograms, each of which is the ratio computed according to what has been just explained, after choosing the hard scale as is indicated in eq. (6.27) (with the green and violet histograms stemming from the first and second options, and the red histograms from the third one). Conversely, the lower part of the main frame presents four ratio plots, where again we subtract one from the actual ratio, so as to have a line at zero in the case of a perfect agreement between the numerator and the denominator. In each plot, the dark blue (orange) histogram corresponds to the ratio of the predictions obtained by dividing the result of cut scenario 1 (scenario 3) by that of cut scenario 2. The symbols are obtained from the histograms of the same colour (with circles and boxes used in the case of the blue and orange colours, respectively), by locally (i.e. bin-by-bin) multiplying the latter by the ratio of the Born cross section that originates from the $\gamma\gamma$ channel over the total Born cross section (which is the sum of those emerging from the $\gamma\gamma$ and $\mu^+\mu^-$ channels) — as will be explained later, the symbols have a more direct connections with physical observables w.r.t. to the corresponding histograms, and will be crucial to establish the fact that the technical cuts are ultimately harmless. Roughly speaking, in a given bin this ratio of Born cross sections is close to one when the two coloured bands at the top of the figure have a similar (dark or light) hue in that bin, and close to zero when the upper coloured band has a much lighter hue than the lower band. The layout of the four plots in the lower part of the main frame that we have just described is identical — they differ in that they correspond to different types of simulations, namely: the upper plot is obtained with the massive calculation in both the numerator and denominator, whereas the three lower plots feature the massless predictions at the numerator and denominator, and differ only by the hard-scale choice.

We start by commenting the results for the pair invariant mass of figure 5, with the left and right panel there obtained with $\sqrt{S} = 3\,\text{TeV}$ and $\sqrt{S} = 10\,\text{TeV}$, respectively. As far as the cross sections are concerned, from the upper coloured band we see that the $\gamma\gamma$-induced one falls by about four (five) orders of magnitude at 3 TeV (10 TeV) when moving from threshold (the left-hand side of the plot) to the kinematic limit (the right-hand side of the plot). Conversely, the total Born cross section (lower coloured band) has a global minimum at about 2 TeV at $\sqrt{S} = 3\,\text{TeV}$ (7 TeV at $\sqrt{S} = 10\,\text{TeV}$), with similar values at the threshold and at the kinematic limit. This implies that, on the whole range, both production mechanisms are essential to obtain sensible predictions, with the $\gamma\gamma$ channel dominant at the threshold (its importance increasing with the c.m. energy), and the $\mu^+\mu^-$ one dominant at the kinematic limit. The three plots in the upper part of the main frame are, up to statistical fluctuations, basically indistinguishable from one another, and all of the histograms there are compatible with being equal to zero. Therefore, we conclude that, regardless of the cut scenario and hard-scale choice, the behaviours of the massive and massless calculations are identical, which is a direct indication that eq. (3.34) is correct.

JHEP10(2025)224

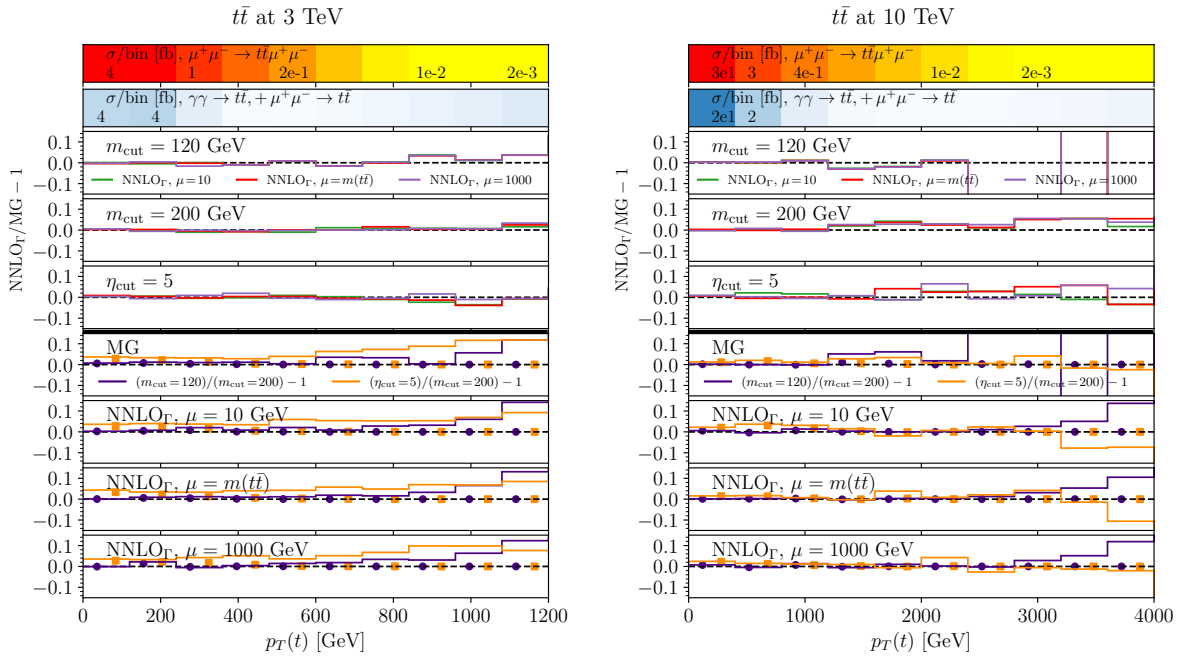

Figure 6. As in figure 5, for the transverse momentum of the top quark.

As far as the four plots in the lower part of the main frame are concerned, the overarching conclusion is that their patterns are identical — again, the massive and the massless calculations behave the same, regardless of the choice of the hard scale in the latter. Having said that, we remark that such patterns, in the case of the histograms at $\sqrt{S} = 3$ TeV, are less trivial than those of the plots in the upper part of the main frame. Specifically, we see that both histograms move away from zero when moving towards the kinematic limit, and that the orange histograms also differ from zero (by $1-2\%$) near threshold. This is the signal of a dependence on the cut scenario adopted. While it has been stressed how these scenarios are rather extreme, this is still a potentially disturbing fact, since it renders it difficult to exclude technical-cut dependences even for sensible choices of such cuts. Fortunately, the dependence we observe is totally irrelevant at the level of physical observables — this is borne out by the fact that the symbols are all compatible with being exactly equal to zero. This can only happen because when the histograms move away from zero (while the symbols are equal to zero), they do so in regions where the $\gamma\gamma$ production channel that underpins them become negligible w.r.t. the $\mu^+\mu^-$ one. Conversely, when the $\gamma\gamma$-channel contributions are non-negligible or dominant, we observe a complete independence of the technical cuts (this is particularly striking when considering the differences between the predictions at $\sqrt{S} = 3$ TeV and $\sqrt{S} = 10$ TeV, with the histograms in the latter case being very close to zero almost on the entire range). Taken together, these two facts give one a crucial message: namely, that while technical cuts are always irrelevant, they are so for basic physics reasons that are process- and observable independent. Namely, their impact is negligible in those kinematic regions where the underlying Born process (from which the would-be singular branching emerges) is initiated by $\gamma\gamma$ fusion. When that impact is visible, the underlying Born process is a $\mu^+\mu^-$-annihilation one. That being the case, the corresponding contribution will be completely swamped by the

JHEP10(2025)224

contributions of genuine $\mu^+\mu^-$ processes, which are both convoluted with the muon PDFs and are perturbatively dominant (i.e. relatively enhanced by a coupling-constant factor).

A corroborating evidence of what we have just said emerges from considering different observables (see e.g. figure 6) and different processes (see appendix A). The same discussion as the one we presented for figure 5 could be repeated in the case of figure 6. What is interesting is to remark that the same conclusions emerge from different mechanisms, in the sense that the $\gamma\gamma$-fusion vs the $\mu^+\mu^-$ annihilation balance is different in the case of the transverse momentum of the top quark, presented in figure 6, w.r.t. to the case of the pair invariant mass discussed before. This is *a fortiori* true for longitudinally-dominated observables such as rapidities, which also follow the same pattern as the one shown explicitly above.

Therefore, the take-home message that should be retained is that the technical cuts are harmless, physics-wise — this renders the procedure advocated in this paper viable, and under firm theoretical control. From the purely technical viewpoint we can also extract another message, namely: in the regions where the technical cuts have a visible effect on the subdominant $\gamma\gamma$ channel, the driving mechanism is that associated with the final-state s-channel branchings, over that stemming from initial-state anti-collinear configurations. This gives one the possibility of addressing the problem in a relatively easy way, since s-channel resonances are more straightforward to address w.r.t. anti-collinear singularities (which have a genuine NNLO topology). It remains true that a solution of this kind will not have any impact on physics predictions.[30] Finally, we remark that what has been done here constitutes a mutual consistency check of the massive-lepton branch of `MadGraph5_aMC@NLO`, and of the non-automated implementation of eqs. (6.5) and (6.15) achieved for the first time during the course of this work.

6.1.2 Choice of factorisation scheme

We now turn to showing the impact of the choice of factorisation scheme, following the formal discussion given in section 5.2. In order to allow for a direct connection with the results shown previously, we shall consider a subset of the same observables as those already analysed in section 6.1.1. Since the issue of scheme dependence has a very direct bearing on phenomenological predictions, the interested reader is urged to check the discussion on this matter which we give in ref. [2].

The factorisation-scheme dependence is assessed by comparing predictions computed in two different factorisation schemes, namely $\overline{\text{MS}}$ [18] and Δ [11]. At variance with what was done in section 6.1.1, such predictions will always be obtained by means of our master formula, eq. (6.12), i.e. with a massless calculation which is of NLO, and is NNLO-improved at its most accurate — in other words, the evolved PDFs are employed, rather than their first-order coefficients, in order to obtain physical predictions. Since the factorisation-scheme dependence grows with energy, we present here the results obtained with $\sqrt{S} = 10\,\text{TeV}$ in order to show the largest effects among those we have studied.

[30] By being sufficiently perverse one can always find a region of the phase space where this is not true any longer. However, as we have shown, such a region will be associated with a cross sections many orders of magnitude smaller than the one at the peak(s).

JHEP10(2025)224

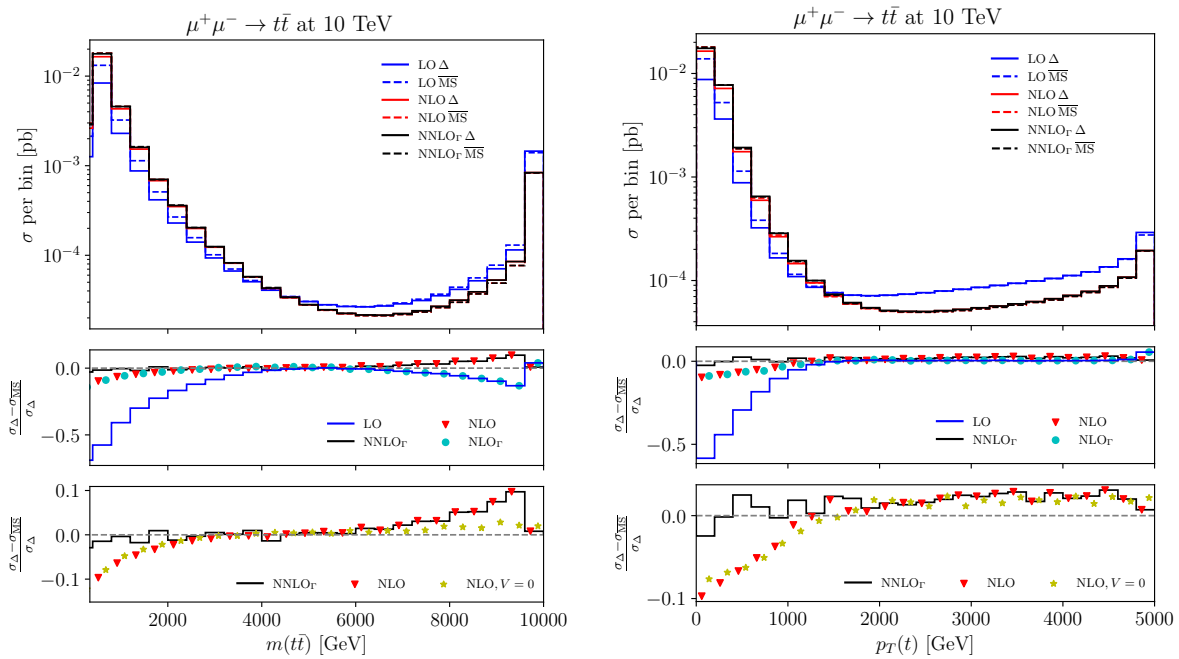

Figure 7. Impact of factorisation-scheme choice on the $t\bar{t}$ invariant mass (left panel), and the transverse momentum of the top quark (right panel), at $\sqrt{S} = 10\,\text{TeV}$. See the text for details.

The results for the pair invariant mass and the single-inclusive transverse momentum in $t\bar{t}$ production are presented in the left and right panel of figure 7, respectively, while analogous observables in W^+W^- production are reported in appendix A (figure 10). All of the plots in these figures have the same layout, as follows. In the main frame the differential cross section (in pb per bin) is shown in absolute value. There are six histograms, which correspond to an increasing level of perturbative accuracy (LO: blue histograms; NLO: red histograms; NNLO: black histograms), and to the two different factorisation-scheme choices (solid histograms: Δ scheme; dashed histograms: $\overline{\rm MS}$ scheme). Below the main frame there are two insets, where the relative differences associated with the factorisation-scheme choice are displayed according to the following definition:

$$\frac{d\sigma_\Delta - d\sigma_{\overline{\rm MS}}}{d\sigma_\Delta}\,, \tag{6.28}$$

which must be understood in a local sense (i.e. the ratio is computed bin-by-bin). The insets have almost identical contents, but the lower one has a reduced range on the y axis, and thus constitutes a zoomed-in view of the upper inset. The results that appear in the insets are relevant to an increasing level of perturbative accuracy, as those in the main frame; specifically, they are all computed by means of eq. (6.28), where the two quantities $d\sigma_\Delta$ and $d\sigma_{\overline{\rm MS}}$ are the solid and dashed histograms, respectively, in the main frame which have the same colour as either the histograms (black for NNLO, and blue for LO) or the symbols (red triangles for NLO) in the insets.[31] Furthermore, there is an additional set of symbols

[31] Symbols rather than histograms are employed in order to improve visibility, given the proximity of the NLO and NNLO predictions.

JHEP10(2025)224

in the upper (blue circles) and lower (yellow stars) insets. The former is equal to NLO_Γ (i.e. it is computed with eq. (6.11) for the NLO corrections), while the latter is identical to the NLO result except for the fact that the finite part of the virtual contribution, defined according to the conventions of ref. [9], is set equal to zero.

We begin by commenting on the predictions for the pair invariant mass (left panel of figure 7). The defining feature of the main frame is the fact that the distribution has two peaks, at the threshold[32] and at the kinematic limit which, as was already pointed out in section 6.1.1, are the results of the dominance of the $\gamma\gamma$ and of the $\mu^+\mu^-$ channel, respectively. We observe that the global maximum (i.e. the highest of the two peaks) changes from that at the right to that at the left when increasing the c.m. energy (e.g. at $\sqrt{S} = 3\,\text{TeV}$ is the one at the right which is highest) — as is known, larger c.m. energies allow the hard process to probe increasingly smaller Bjorken x's, where the photon density grows fast. The relative heights of the two peaks also change with the perturbative precision at a given c.m. energy, with the one at threshold (at the kinematic limit) higher (lower) at the NLO(NNLO) w.r.t. the LO result. In general, the changes induced by the inclusion of higher-order corrections are *very* significant, and such corrections are therefore essential in order to obtain sensible physical predictions. This is reflected on the topic which is our primary interest here, namely the factorisation-scheme dependence, whose actual size is best seen in the insets. At the LO, such a fractional dependence is extremely large, and grows with the c.m. energy. It is largest at the threshold, where the ratio of eq. (6.28) is equal to -30% and -60% at $\sqrt{S} = 3\,\text{TeV}$ and $\sqrt{S} = 10\,\text{TeV}$, respectively. The reduction of these fractions when including the δNLO and the approximate δNNLO corrections is impressive. Specifically, at the NLO one obtains -5% and -10% at the threshold at the two c.m. energies, and this is further reduced at the NNLO to being statistically compatible with zero — this is entirely due to the cancellation mechanism explained in section 5.2, and it is a very direct confirmation that our NNLO-improved cross section of eq. (6.15) works as we envisage it to do in the regions dominated by the $\gamma\gamma$ channel. Such a dominance can be immediately understood by observing the almost perfect agreement between the NLO and NLO_Γ predictions (red triangles and blue circles, respectively) on the left side of the figure. Conversely, we note that in the kinematic-limit region a visible factorisation-scheme dependence remains. In that respect, we observe that, firstly, our NNLO improvement has no impact there, since that region is a $\mu^+\mu^-$-dominated one; and, secondly, that this effect is almost entirely due to the virtual corrections, which are very large — one must bear in mind that NLO-driven factorisation-scheme dependences (as is the case of the virtuals here) can only be cancelled at the NNLO, and in the kinematic-limit region we do not include any sizeable contribution of that order. Indeed, this is shown clearly by the fact that when such virtual corrections are set equal to zero, one finds an almost perfect cancellation of factorisation-scheme effects also when approaching the kinematic limit (the yellow symbols are close to zero there). While of course switching virtual corrections off is an unphysical operation, we point out that the bulk of the NNLO scheme-compensating terms can in fact be predicted (essentially, they are equal to the virtual matrix elements convoluted with the K_{ij} functions), and if need be they could be included in order to reduce the theoretical

[32]The fact that the leftmost bin is lower than the bin to its right is simply due to the fact that its left border is smaller than the actual $t\bar{t}$ mass threshold.

JHEP10(2025)224

systematics. This is not an entirely satisfactory solution, since it leaves out other terms that are perturbatively on the same footing as those one would include. A better approach is to use the theoretical argument that, in the kinematic regions dominated by large Bjorken x's, the Δ scheme [11] is superior to the $\overline{\rm MS}$ one — for example, Δ never introduces the double logarithms of $(1-z)$ which are present in $\overline{\rm MS}$ in both the PDFs and the short-distance cross sections, and which are eventually cancelled in physical observables. An unpleasant by-product of this fact is that, in order to obtain distributions of comparable smoothness in $\overline{\rm MS}$- and Δ-based runs, one must use a statistical sample several times larger in the former case w.r.t. the latter one (this factor being approximately equal to five at $\sqrt{S}=10\,\text{GeV}$). The interested reader can find extensive discussions on this point in ref. [12], but should note that here the problem is much more severe, owing to the vastly larger c.m. energies w.r.t. those of relevance to the studies of ref. [12].

Most of what has been said about the pair invariant mass applies to the case of the top-quark transverse momentum distribution, shown in right panel of figure 7. We remark again the change in the prominence of the peak, with the one at the left end of the spectrum increasingly dominant with increasing c.m. energy w.r.t. the one at the right end of the spectrum. That is, one passes from a large-x, $\mu^+\mu^-$-dominated configuration to a small-x, $\gamma\gamma$-dominated one. Again there is an extremely large factorisation-scheme dependence at the LO, which is significantly reduced when δNLO, and especially approximated δNNLO, corrections are included — as was the case for the pair invariant mass, this is most evident on the left side of the distribution. Conversely, the residual scheme dependence in the kinematic-limit region is smaller than in the case of the pair invariant mass, and this is due to the fact that the distribution here is less peaked than there, which dilutes the impact of the virtual corrections; this is demonstrated by the fact that setting these corrections equal to zero has a much smaller effect than for the pair invariant mass at the kinematic limit.

7 Conclusions

The main achievement of this paper is the definition of a process- and observable-independent contribution of NNLO, which can be added to any NLO-accurate prediction emerging from the collinear factorisation theorem, and which improves the latter in regions dominated by vector-boson fusion, thus including those associated with VBF topologies. Specifically, such an NNLO contribution is given in eq. (6.5), which must be used as is prescribed by eqs. (6.14) and (6.15); in the latter equation, these NNLO results are summed to those of an NLO computation of the $2\to m$ lepton-collision process of interest. In order for this final section to be as self-contained as is possible, we re-write those key equations here: our physical predictions correspond to the l.h.s. of eq. (6.15)

$$\begin{aligned}d\sigma(P_1,P_2)=&\,d\zeta_1\,d\zeta_2\sum_{ij}\Gamma_{i/\ell}(\zeta_1)\Gamma_{j/\ell}(\zeta_1)\\&\times\left(d\hat{\sigma}^{[0]}_{ij}(\zeta_1P_1,\zeta_2P_2)+\frac{\alpha}{2\pi}d\hat{\sigma}^{[1]}_{ij}(\zeta_1P_1,\zeta_2P_2)+\delta_{i\ell}\delta_{j\ell}\left(\frac{\alpha}{2\pi}\right)^2d\hat{\sigma}^{[2]}_{\delta\text{NNLO}_\Gamma}(\zeta_1P_1,\zeta_2P_2)\right),\end{aligned}\tag{7.1}$$

JHEP10(2025)224

where the momenta of the beam muons are now denoted by uppercase symbols (P_i), and the contribution of NNLO that we have obtained in this work is normalised as follows:

$$\left(\frac{\alpha}{2\pi}\right)^2 d\hat{\sigma}^{[2]}_{\delta\text{NNLO}_\Gamma}(p_1,p_2) = d\hat{\Sigma}_{\delta\text{NNLO}_\Gamma}(p_1,p_2)\,, \tag{7.2}$$

where its short-distance cross section is defined thus:

$$\begin{aligned} d\hat{\Sigma}_{\delta\text{NNLO}_\Gamma}(p_1,p_2) = {} & \left(\frac{1}{1-y_1}\right)_{\delta_\text{I}} \left(\frac{1}{1-y_2}\right)_{\delta_\text{I}} \Big((1-y_1)(1-y_2)\mathcal{M}^{(m+2)}_{\ell\ell}\Big)\, d\phi_{m+2}(p_1,p_2) \\ & + \frac{\alpha}{2\pi}\,\mathcal{Q}^{(\delta_\text{I})'}_{\gamma\ell}(z_2) \left(\frac{1}{1-y_1}\right)_{\delta_\text{I}} \Big((1-y_1)\mathcal{M}^{(m+1)}_{\ell\gamma}\Big)\, d\phi_{m+1}(p_1,z_2p_2)\, dz_2 \\ & + \frac{\alpha}{2\pi}\,\mathcal{Q}^{(\delta_\text{I})'}_{\gamma\ell}(z_1) \left(\frac{1}{1-y_2}\right)_{\delta_\text{I}} \Big((1-y_2)\mathcal{M}^{(m+1)}_{\gamma\ell}\Big)\, d\phi_{m+1}(z_1p_1,p_2)\, dz_1 \\ & + \left(\frac{\alpha}{2\pi}\right)^2 \mathcal{Q}^{(\delta_\text{I})'}_{\gamma\ell}(z_1)\,\mathcal{Q}^{(\delta_\text{I})'}_{\gamma\ell}(z_2)\mathcal{M}^{(m)}_{\gamma\gamma}\, d\phi_m(z_1p_1,z_2p_2)\, dz_1\, dz_2\,. \end{aligned} \tag{7.3}$$

The contribution of eq. (7.3) to eq. (7.1) constitutes the improvement of NNLO mentioned at the beginning of this section, while the NLO predictions appear in the second line of the latter equation. As was said, we expect this improvement to be particularly accurate in the kinematic regions dominated by VBF-like configurations or, more generally, by underlying partonic collisions stemming from the $\gamma\gamma$ channel. Equation (7.3) features the $2 \to 2+m$ matrix elements that allow one to retain exactly both logarithmic and power-suppressed effects in the mass of the Z boson, as well as all of those due to the Z/γ interference. At the same time, this formalism resums all light-fermion mass effects through the usage of lepton PDFs, at the logarithmic accuracy to which such PDFs are available. The PDFs must not include weak massive vector bosons in their partonic contents.

While of NNLO, eq. (7.3) is *not* a complete NNLO cross section, as is also underscored by the restrictions on the sums over parton types in eq. (7.1) which are enforced by the Kronecker delta's. It cannot thus have the same level of accuracy as that of complete NNLO predictions, but it has the advantage of being fairly easy to calculate, essentially implying the same level of computational complexity as the corresponding NLO cross section. Therefore, it can easily be automated, although this is something that we have not yet considered. More importantly, it gives one a viable, and theoretically vastly superior, alternative to the usage of weak-boson PDFs, which is correctly defined in the whole of the phase space, with a straightforward inclusion of higher logarithmic and fixed-order contributions, a well-defined theoretical systematics, and the complete control over theoretical uncertainties.

A number of immediate phenomenological consequences of the results presented here are discussed in a companion paper [2].

Acknowledgments

We thank Giovanni Stagnitto for having provided us with a still-unreleased NLL- and NLO-accurate version of the muon PDFs of ref. [6]. DP and MZ acknowledge the financial support by the MUR (Italy), with funds of the European Union (NextGenerationEU), through the PRIN2022 grant 2022EZ3S3F; likewise FM, through the PRIN2022 grant 2022RXEZCJ. SF thanks the TH division of CERN for the hospitality during the course of this work.

JHEP10(2025)224

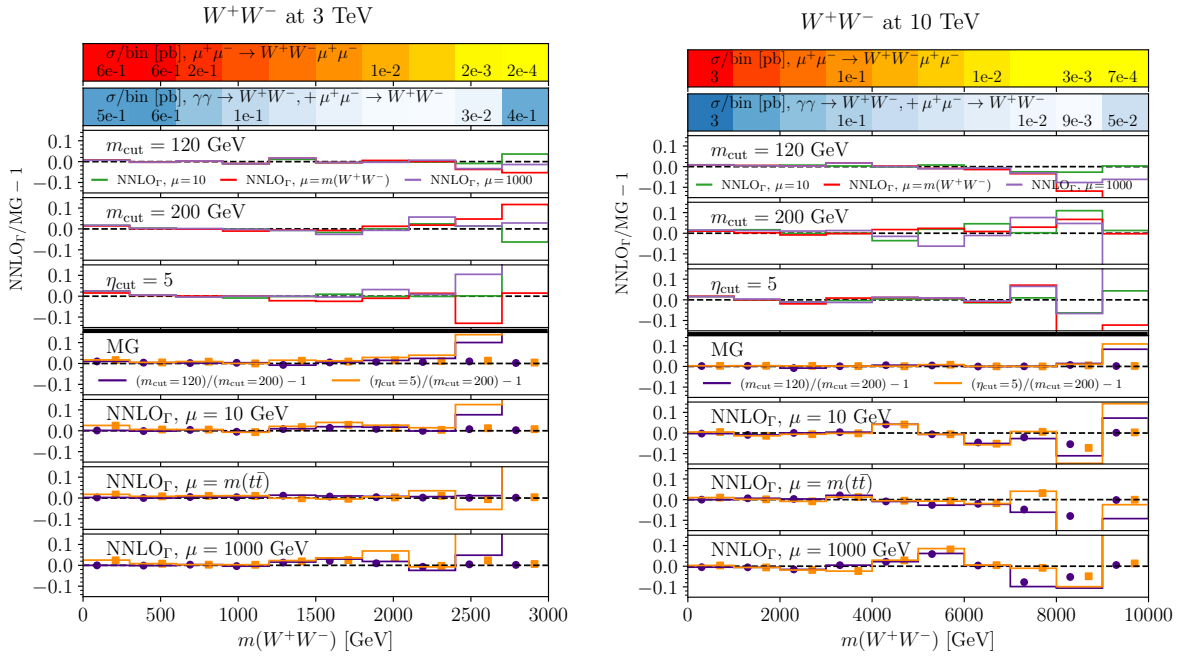

Figure 8. As in figure 5, for W^+W^- production.

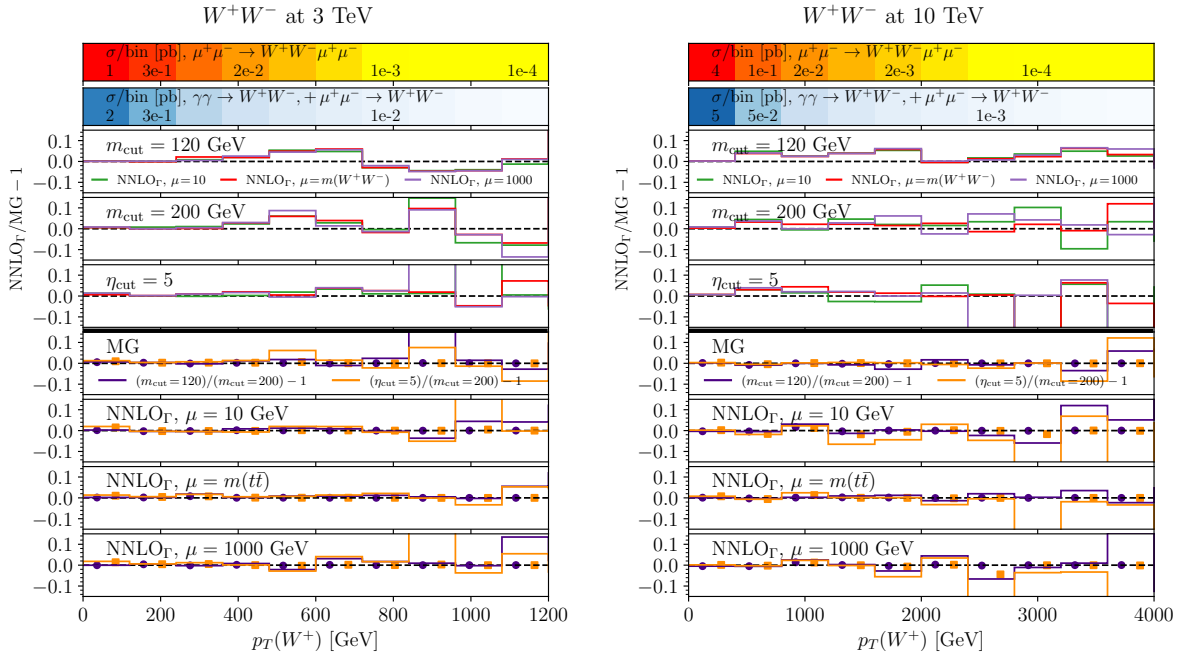

Figure 9. As in figure 6, for W^+W^- production.

A Additional plots

In this appendix we present the analogues of the plots shown in section 6.1.1 and 6.1.2, obtained when considering W^+W^- production rather than $t\bar{t}$ production as was done in the main text.

JHEP10(2025)224

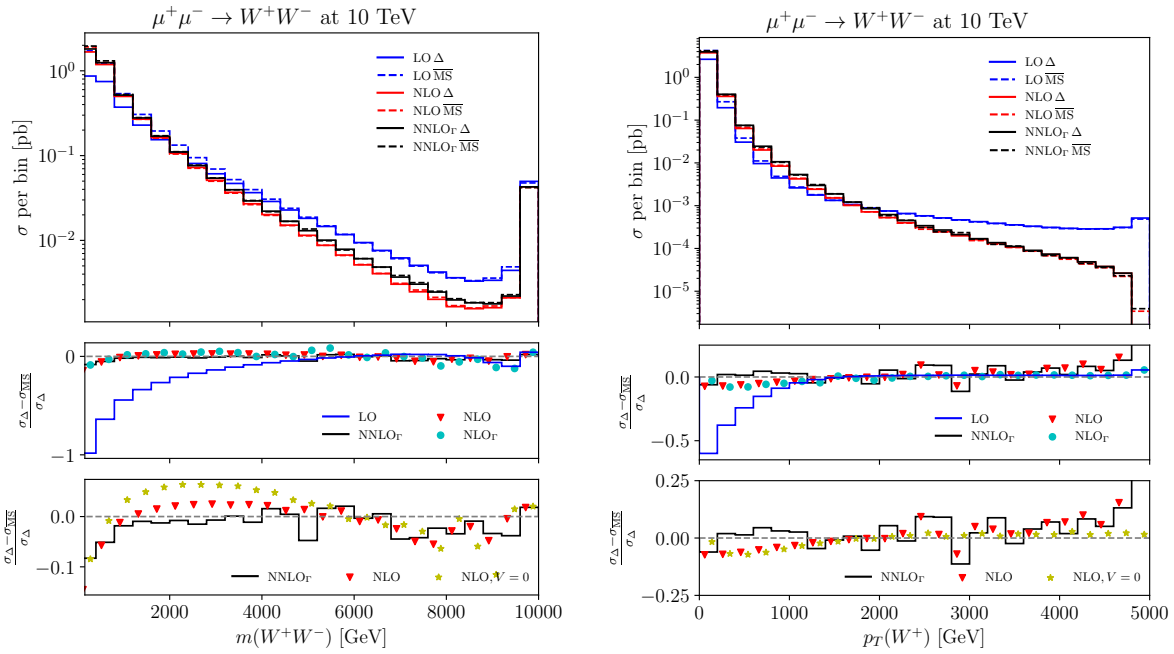

Figure 10. As in figure 7, for W^+W^- production.

The take-home message is that, despite the significant differences in the production mechanisms of W^+W^- and $t\bar{t}$ pairs, the conclusions about the dependences on the technical cuts and on the factorisation-scheme choice are exactly the same. As we have argued in the text, this is far from being accidental, and is rather the consequence of the physics which underpins the procedure we have constructed (in addition to constituting a check that such a procedure has been correctly implemented in a computer code).

B An FKS-type phase space for double-real contributions

The implementation of eq. (7.3) is independent of that of the NLO cross section used to obtain phenomenological predictions, since the two are now uncorrelated. Having said that, it is convenient for us to adopt also in the case of eq. (7.3) a phase-space parametrisation analogous to that we employ in our NLO computations, namely one based on the FKS formalism. With the momentum assignments of eq. (3.1), we can write:[33]

$$\begin{aligned} d\phi_{m+2} &\equiv d\phi_{m+2}\left(p_1+p_2;k_1,k_2,\{T_i\}_{i=1}^m\right) \\ &= (2\pi)^4\delta\left(p_1+p_2-k_1-k_2-\sum_{i=1}^m T_i\right)\prod_{j=1}^2\frac{d^3k_j}{(2\pi)^3 2k_j^0}\prod_{i=1}^m\frac{d^3T_i}{(2\pi)^3 2T_i^0}\,. \end{aligned} \tag{B.1}$$

With

$$s=(p_1+p_2)^2 \tag{B.2}$$

[33] The particles of the set of the tagged objects and their momenta are denoted by the same symbols (T_i) here, since no confusion is possible.

JHEP10(2025)224

and the FKS-type parametrisations in the $\ell^+\ell^-$ cm frame:[34]

$$k_j = \frac{\sqrt{s}}{2}\xi_j \left(1, \sqrt{1-y_j^2}\vec{e}_{Tj}, (-)^{j-1}y_j\right) , \tag{B.3}$$

where

$$\vec{e}_{Tj} = (\sin\varphi_j, \cos\varphi_j) . \tag{B.4}$$

Then:

$$\begin{aligned} d\phi_{m+2} = &\left(\frac{s}{8(2\pi)^3}\right)^2 \xi_1 d\xi_1 dy_1 d\varphi_1 \xi_2 d\xi_2 dy_2 d\varphi_2 \\ &\times d\phi_m \left(p_1 + p_2 - k_1 - k_2; \{T_i\}_{i=1}^m\right) . \end{aligned} \tag{B.5}$$

The quantity on the second line of eq. (B.5) is a proper m-body phase space, where the four vector $p_1 + p_2 - k_1 - k_2$ is thought to be given; as such, it can be defined as it is most convenient. The variables $y_{1,2}$ coincide with their namesakes in eq. (3.34), while we shall take $z_{1,2} = 1 - \xi_{1,2}$ (bear in mind that both of these apply solely to the NNLO-type contributions). It is a matter of simple algebra to arrive at:

$$\left(\sum_{i=1}^m T_i\right)^2 \equiv (p_1 + p_2 - k_1 - k_2)^2 = s + \frac{s}{2}\xi_1\xi_2(1-\Omega) - s(\xi_1+\xi_2) \geq M_{\rm INF}^2 , \tag{B.6}$$

with $M_{\rm INF}^2$ the lower bound on the invariant mass squared of the T system, and

$$\Omega = \sqrt{1-y_1^2}\sqrt{1-y_2^2}\,\vec{e}_{T1}\cdot\vec{e}_{T2} - y_1 y_2 \quad \Longrightarrow \quad -1 \leq \Omega \leq 1 . \tag{B.7}$$

Equation (B.6) leads to

$$0 \leq \xi_1 \leq 1 - \hat{M}_{\rm INF}^2 , \qquad 0 \leq \xi_2 \leq \frac{2(1-\hat{M}_{\rm INF}^2 - \xi_1)}{2 - (1-\Omega)\xi_1} , \tag{B.8}$$

where we have defined:

$$\hat{M}_{\rm INF}^2 = \frac{M_{\rm INF}^2}{s} . \tag{B.9}$$

Note that:

$$\frac{2(1-\hat{M}_{\rm INF}^2 - \xi_1)}{2 - (1-\Omega)\xi_1} \leq 1 - \hat{M}_{\rm INF}^2 . \tag{B.10}$$

A possible procedure is then the following:

- Generate $-1 \leq y_{1,2} \leq 1$ and $0 \leq \varphi_{1,2} \leq 2\pi$.
- Generate $\xi_{1,2}$ in the ranges of eq. (B.8).
- With the above, construct k_1 and k_2, and thus $p_1 + p_2 - k_1 - k_2$.

[34] According to eq. (3.34), $k_2 \parallel p_2$ when $y_2 = 1$, whence the sign of the third spatial component in eq. (B.3).

JHEP10(2025)224

- In the rest frame of $p_1+p_2-k_1-k_2$ generate the m T_i momenta; boost them back to the p_1+p_2 rest frame.

The generation of $\xi_{1,2}$ requires the prior knowledge of $M^2_{\rm INF}$. This is typically a constant (e.g. $4m_W^2$ for W^+W^- production). However, for processes with $m \geq 3$, it is conceivable that one of the variables that parametrise $d\phi_m$ be equal to the invariant mass squared of the T system. If so, one can generate this variable before the generation of $\xi_{1,2}$, and then proceed as is written above; the last step would entail the generation of the remaining $3m-5$ variables for $d\phi_m$.

The parametrisation defined above works also for a one-body system (i.e. for $m=1$). However, in that special case the inequality in eq. (B.6) becomes an equality, and $M^2_{\rm INF}=m^2_{T_1}$, with m_{T_1} the invariant mass of the final state particle (e.g. the Higgs). This equality is formally enforced by the fact that now:

$$\begin{aligned} d\phi_1\left(p_1+p_2-k_1-k_2;T_1\right) &= (2\pi)^4\delta(p_1+p_2-k_1-k_2-T_1) \\ &\quad\times\frac{d^4T_1}{(2\pi)^3}\,\delta\Big(T_1^2-m^2_{T_1}\Big) \qquad\qquad (B.11)\\ &= (2\pi)\delta\bigg(s+\frac{s}{2}\xi_1\xi_2(1-\Omega)-s(\xi_1+\xi_2)-m^2_{T_1}\bigg)\,. \qquad\qquad (B.12)\end{aligned}$$

Equation (B.12) allows one to trivially integrate out either ξ_1 or ξ_2, and to restore the correct counting of independent phase-space variables (with a one-body system, there must be 5 independent variables, but eq. (B.5) has a 6-dimensional measure). Instead of eq. (B.8) we thus have:

$$0\leq\xi_1\leq 1-m^2_{T_1}/s\,,\qquad \xi_2=\bar{\xi}_2\equiv\frac{2(1-m^2_{T_1}/s-\xi_1)}{2-(1-\Omega)\xi_1}\,, \qquad (B.13)$$

and

$$d\phi_1\left(p_1+p_2-k_1-k_2;T_1\right)=\frac{2(2\pi)}{s(2-(1-\Omega)\xi_1)}\,\delta(\xi_2-\bar{\xi}_2)\,. \qquad (B.14)$$

The slightly unpleasant feature of eq. (B.8), and of eqs. (B.13) and (B.14), is the asymmetric role played by ξ_1 and ξ_2. Although this does not necessarily imply a poor numerical behaviour, one can possibly interchange the roles of these two variables in a random manner. Alternatively, one can proceed by following one of the two approaches we are now going to describe.

In the first approach, we define

$$\varsigma=\xi_1+\xi_2\,,\qquad \delta=\xi_1-\xi_2\,, \qquad (B.15)$$

so that

$$\xi_1=\frac{1}{2}(\varsigma+\delta)\,,\qquad \xi_2=\frac{1}{2}(\varsigma-\delta)\,, \qquad (B.16)$$

and

$$d\xi_1 d\xi_2=\frac{1}{2}d\varsigma d\delta\,. \qquad (B.17)$$

The region of integration in the $\langle\varsigma,\delta\rangle$ plane can be found be imposing $\xi_i\geq 0$, $\xi_i\leq 1$, and the condition of eq. (B.6). The borders of these regions are depicted in figure 11 as thick blue lines,

JHEP10(2025)224

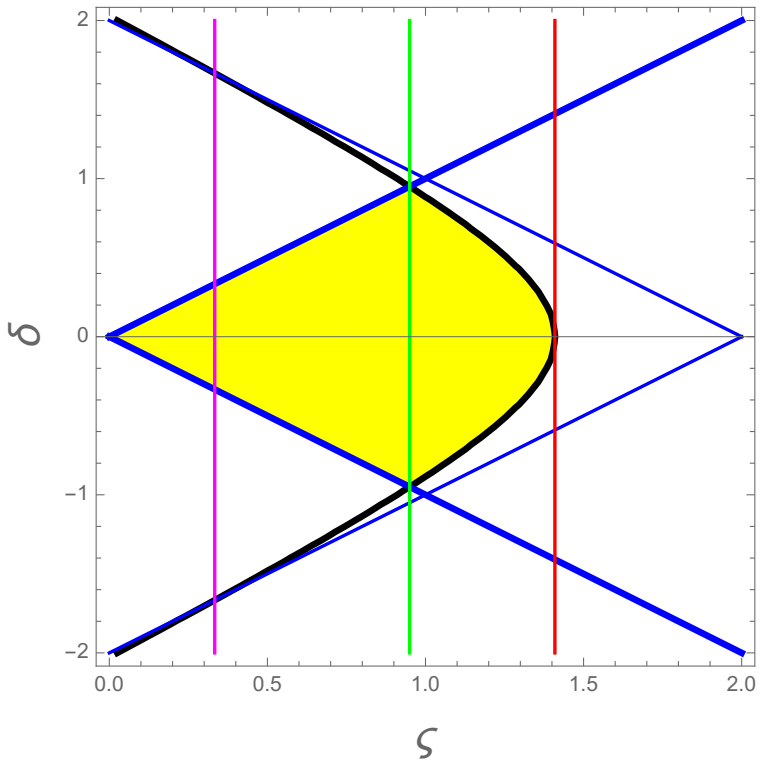

Figure 11. Integration region for the variables of eq. (B.15), having set $\Omega = -0.85$ and $\hat{M}^2_{\rm INF} = 0.05$.

thin blue lines, and a thick black line respectively; the resulting overlapping region, i.e. the sought region of integration, is shown in yellow. It turns out to be convenient to first integrate in δ and then in ς. Thus, the upper branch ($\delta \geq 0$) of the black line of figure 11 is given by

$$\Delta(\varsigma) = \sqrt{\frac{8(1-\hat{M}^2_{\rm INF}) - 8\varsigma + (1-\Omega)\varsigma^2}{1-\Omega}}\,. \tag{B.18}$$

As is shown in the figure, the function will be relevant in $\varsigma_1 \leq \varsigma \leq \varsigma_2$, where

$$\varsigma_1 = 1 - \hat{M}^2_{\rm INF}\,, \tag{B.19}$$

$$\varsigma_2 = \frac{4 - 2\sqrt{2}\sqrt{1+\Omega+\hat{M}^2_{\rm INF}(1-\Omega)}}{1-\Omega}\,, \tag{B.20}$$

whose values are shown as green and red lines in figure 11. By construction:

$$\Delta(\varsigma_1) = \varsigma_1\,, \tag{B.21}$$

$$\Delta(\varsigma_2) = 0\,. \tag{B.22}$$

We note that $\varsigma_2 \geq \varsigma_1$, and that:

$$\lim_{\Omega\to 1} \varsigma_2 = \varsigma_1\,, \tag{B.23}$$

which implies that the integral of any function regular in $\varsigma_1 \leq \varsigma \leq \varsigma_2$ will vanish for $\Omega \to 1$. Furthermore, by defining ς_0 so that

$$\Delta(\varsigma_0) = 2 - \varsigma_0\,, \tag{B.24}$$

JHEP10(2025)224

(whose value is shown as a magenta line in figure 11) we have

$$\varsigma_0 < \varsigma_1 < 1\,, \qquad \varsigma_2 < 2\,, \tag{B.25}$$

for any $\hat{M}^2_{\rm INF} > 0$. This implies that the conditions stemming from requiring $\xi_i \leq 1$ are never relevant for the determination of the integration region. So finally we have that:

$$\begin{aligned}&\int d\xi_1 \Theta\left(\xi_2 \leq 1-\hat{M}^2_{\rm INF}\right) \int d\xi_2 \Theta\left(\xi_2 \leq \frac{2(1-\hat{M}^2_{\rm INF}-\xi_1)}{2-(1-\Omega)\xi_1)}\right) f(\xi_1,\xi_2) \\ &= \frac{1}{2}\int_0^{\varsigma_1} d\varsigma \int_{-\varsigma}^{\varsigma} d\delta f\left(\frac{\varsigma+\delta}{2}, \frac{\varsigma-\delta}{2}\right) + \frac{1}{2}\int_{\varsigma_1}^{\varsigma_2} d\varsigma \int_{-\Delta(\varsigma)}^{\Delta(\varsigma)} d\delta f\left(\frac{\varsigma+\delta}{2}, \frac{\varsigma-\delta}{2}\right)\end{aligned} \tag{B.26}$$

for any function $f(\xi_1, \xi_2)$. We have verified eq. (B.26) numerically for different choices of f, and analytically for $f \equiv 1$.

We now turn to discussing the second approach, based on two variables that we denote by λ and t, which are such that:

$$\xi_1 = \lambda t\,, \qquad \xi_2 = \lambda(1-t)\,, \tag{B.27}$$

with

$$d\xi_1 d\xi_2 = \lambda d\lambda dt\,. \tag{B.28}$$

As was done before, the region of integration in the $\langle \lambda, t\rangle$ plane can be found be imposing $\xi_i \geq 0$, $\xi_i \leq 1$, and the condition of eq. (B.6). The borders of these regions are depicted in figure 11 as thick blue lines, thin blue lines, and a thick black line respectively; the resulting overlapping region, i.e. the sought region of integration, is shown in yellow. As was already the case, the conditions stemming from $\xi_i \leq 1$ are irrelevant, and the only non-trivial constraint is due to eq. (B.6). In the present case, the best strategy is that of integrating first in λ and then in t; thus, the black line of figure 12 is given by:

$$\Lambda(t) = \frac{1-\sqrt{1-2(1-\hat{M}^2_{\rm INF})(1-\Omega)(1-t)t}}{(1-\Omega)(1-t)t}. \tag{B.29}$$

We note that:

$$\lim_{t\to 0}\Lambda(t) = \lim_{t\to 1}\Lambda(t) = \lim_{\Omega\to 1}\Lambda(t) = 1-\hat{M}^2_{\rm INF}\,. \tag{B.30}$$

When $t \simeq 0$, and/or $t \simeq 1$, and/or $\Omega \simeq 1$ a numerical 0/0 result in the evaluation of $\Lambda(t)$ can be avoided by using the following series expansion:

$$\Lambda(t) = (1-\hat{M}^2_{\rm INF})\sum_{k=0}^{\infty}\widehat{\Lambda}_k R^k\,, \qquad R = (1-\hat{M}^2_{\rm INF})(1-\Omega)(1-t)t\,, \tag{B.31}$$

with

$$\widehat{\Lambda}_k = 1, \frac{1}{2}, \frac{1}{2}, \frac{5}{8}, \frac{7}{8}, \frac{21}{16}, \ldots \tag{B.32}$$

JHEP10(2025)224

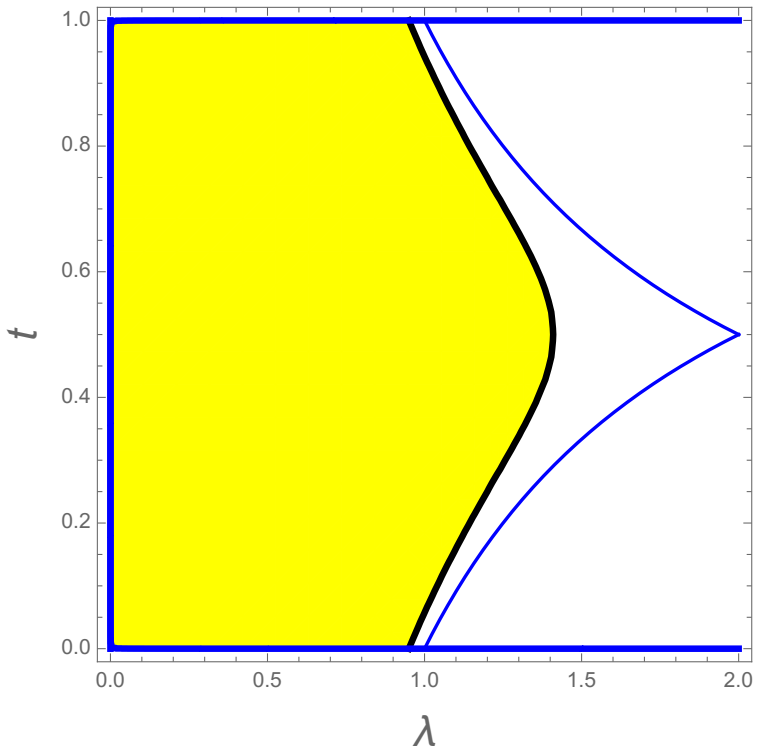

Figure 12. Integration region for the variables of eq. (B.27), having set $\Omega = -0.85$ and $\hat{M}^2_{\text{INF}} = 0.05$.

This expansion is quite accurate: by retaining its first six terms whose coefficients are given here, the relative difference between $\Lambda(t)$ and its truncated expansion is smaller than 10^{-5} for $R \leq 0.1$. Finally:

$$\int d\xi_1 \Theta\Big(\xi_2 \leq 1 - \hat{M}^2_{\text{INF}}\Big) \int d\xi_2 \Theta\left(\xi_2 \leq \frac{2(1 - \hat{M}^2_{\text{INF}} - \xi_1)}{2 - (1-\Omega)\xi_1)}\right) f(\xi_1, \xi_2)$$
$$= \int_0^1 dt \int_0^{\Lambda(t)} d\lambda\, \lambda\, f\left(\lambda t, \lambda(1-t)\right)) \,. \tag{B.33}$$

We have verified eq. (B.33) numerically for $f \equiv 1$ and several values of Ω and $\hat{M}^2_{\text{INF}}$.

C Azimuthal correlations

As is known, a local collinear counterterm requires an additional contribution w.r.t. the standard Altarelli-Parisi kernel when the off-shell parton that participates in the branching has spin one; such a contribution has a non-trivial dependence on the azimuthal angle, and because of this it is essential to obtain a stable numerical behaviour, in spite of the fact that it integrates to zero — more details on this in the context of the FKS subtraction can be found in refs. [9, 13].

VBF topologies feature two t-channel photon exchanges, and therefore there will be two azimuthal kernels (one for each of the photons) to be included. As was stressed multiple times in the main text, in such topologies the collinear limits are incoherent, and one can thus arrive at the final result by iterating the one relevant to a single branching.

JHEP10(2025)224

The quantity of interest is the matrix element of the process of eq. (3.2), in the collinear limits $p_1 \parallel k_1$ and $p_2 \parallel k_2$. Following the procedure of appendix B of ref. [9], we write

$$\mathcal{M}_{\ell\ell}^{(m+2)} = \sum_{h_1 g_1} \sum_{h_2 g_2} \left| \mathcal{A}_{\ell\ell}^{(m+2)}(h_1, g_1; h_2, g_2) \right|^2 , \tag{C.1}$$

$$\mathcal{A}_{\ell\ell}^{(m+2)}(h_1, g_1; h_2, g_2) \overset{p_1 \| k_1, p_2 \| k_2}{\longrightarrow} e^2 \sum_{f_1 f_2} \mathcal{A}_{\gamma\gamma}^{(m)}(f_1; f_2) S_{\gamma\ell}^{f_1 h_1 g_1}(z_1) S_{\gamma\ell}^{f_2 h_2 g_2}(z_2) . \tag{C.2}$$

We have denoted by h_i (g_i) the helicity of the incoming (outgoing) lepton with momentum p_i (k_i), and by f_i the polarisation index of the photon emitted in the branching of leg i. In other words, the amplitude relevant to the branching process

$$\ell(p_i, h_i) \longrightarrow \ell(k_i, g_i) + \gamma(p_i - k_i, f_i) \equiv \ell((1 - z_i)p_i, g_i) + \gamma(z_i p_i, f_i) , \tag{C.3}$$

has been denoted by

$$S_{\gamma\ell}^{f_i h_i g_i}(z_i) . \tag{C.4}$$

By squaring the r.h.s. of eq. (C.2) we simplify the result by using the relationships between the branching amplitudes and the splitting kernels, per ref. [9]:

$$\sum_{h_i g_i} \left| S_{\gamma\ell}^{+ h_i g_i}(z_i) \right| = \sum_{h_i g_i} \left| S_{\gamma\ell}^{- h_i g_i}(z_i) \right| = \frac{1}{2 p_i \cdot k_i} P_{\gamma\ell}^{<}(z_i) , \tag{C.5}$$

$$\sum_{h_i g_i} S_{\gamma\ell}^{+ h_i g_i}(z_i) \left(S_{\gamma\ell}^{- h_i g_i}(z_i) \right)^\star = \frac{1}{4 p_i \cdot k_i} \frac{\langle p_i k_i \rangle}{[p_i k_i]} Q_{\gamma^\star \ell}(z_i) , \tag{C.6}$$

whence we obtain:

$$\begin{aligned} \mathcal{M}_{\ell\ell}^{(m+2)} \overset{p_1 \| k_1, p_2 \| k_2}{\longrightarrow} \frac{(4\pi\alpha)^2}{(p_1 \cdot k_1)(p_2 \cdot k_2)} \Big[& P_{\gamma\ell}^{<}(z_1) P_{\gamma\ell}^{<}(z_2) \mathcal{M}_{\gamma\gamma}^{(m)} + P_{\gamma\ell}^{<}(z_1) Q_{\gamma^\star \ell}(z_2) \widetilde{\mathcal{M}}_{\gamma\gamma^\star}^{(m)} \\ & + Q_{\gamma^\star \ell}(z_1) P_{\gamma\ell}^{<}(z_2) \widetilde{\mathcal{M}}_{\gamma^\star\gamma}^{(m)} + Q_{\gamma^\star \ell}(z_1) Q_{\gamma^\star \ell}(z_2) \widetilde{\mathcal{M}}_{\gamma^\star\gamma^\star}^{(m)} \Big] , \end{aligned} \tag{C.7}$$

where $\mathcal{M}_{\gamma\gamma}^{(m)}$ is the matrix element for the process of eq. (3.37), which is ubiquitous in the text, and we have defined:

$$\widetilde{\mathcal{M}}_{\gamma\gamma^\star}^{(m)} = \Re \left[\sum_{f_1} \mathcal{A}_{\gamma\gamma}^{(m)}(f_1; +) \left(\mathcal{A}_{\gamma\gamma}^{(m)}(f_1; -) \right)^* \frac{\langle p_2 k_2 \rangle}{[p_2 k_2]} \right] , \tag{C.8}$$

$$\widetilde{\mathcal{M}}_{\gamma^\star\gamma}^{(m)} = \Re \left[\sum_{f_2} \mathcal{A}_{\gamma\gamma}^{(m)}(+; f_2) \left(\mathcal{A}_{\gamma\gamma}^{(m)}(-; f_2) \right)^* \frac{\langle p_1 k_1 \rangle}{[p_1 k_1]} \right] , \tag{C.9}$$

$$\begin{aligned} \widetilde{\mathcal{M}}_{\gamma^\star\gamma^\star}^{(m)} = & \frac{1}{2} \Re \left[\mathcal{A}_{\gamma\gamma}^{(m)}(+; +) \left(\mathcal{A}_{\gamma\gamma}^{(m)}(-; -) \right)^* \frac{\langle p_1 k_1 \rangle}{[p_1 k_1]} \frac{\langle p_2 k_2 \rangle}{[p_2 k_2]} \right] \\ & + \frac{1}{2} \Re \left[\mathcal{A}_{\gamma\gamma}^{(m)}(+; -) \left(\mathcal{A}_{\gamma\gamma}^{(m)}(-; +) \right)^* \frac{\langle p_1 k_1 \rangle}{[p_1 k_1]} \frac{[p_2 k_2]}{\langle p_2 k_2 \rangle} \right] . \end{aligned} \tag{C.10}$$

JHEP10(2025)224

We point out that the matrix elements of eqs. (C.8) and (C.9) coincide with the standard $\widetilde{\mathcal{M}}$ of FKS implementations; the new notation only helps one understand which of the two legs that undergo a collinear splitting induces azimuthal correlations.

If one adopts the language of dipole subtraction [19] instead, for a single collinear lepton splitting one finds:

$$|\mathcal{A}_\ell||^2 = \frac{8\pi\alpha}{-k^2}\left(\mathcal{A}_\gamma\mathcal{A}_\gamma^\star\right)^{\rho\sigma}\left[-g_{\rho\sigma}z + \frac{4(1-z)}{z}\hat{k}_\rho^\perp\hat{k}_\sigma^\perp\right]. \tag{C.11}$$

Here, k is the momentum of the photon that emerges from the lepton branching. With FKS variables, $k^2 = -s\xi(1-y)/2$, and $z = 1-\xi$. Furthermore, $\left(\mathcal{A}_\gamma\mathcal{A}_\gamma^\star\right)^{\rho\sigma}$ would be the squared amplitude for the process where the lepton line is replaced by an on-shell photon, if it were summed over photon polarisations. Finally, $\hat{k}^\perp = (0, \cos\phi, \sin\phi, 0)$. With this, we can iterate eq. (C.11), and obtain the analogue of eq. (C.7), which reads as follows:

$$\begin{aligned}\mathcal{M}_{\ell\ell}^{(m+2)} \xrightarrow{p_1\|k_1,p_2\|k_2} & \frac{(4\pi\alpha)^2}{(p_1\cdot k_1)(p_2\cdot k_2)}\left(\mathcal{A}_{\gamma\gamma}\mathcal{A}_{\gamma\gamma}^\star\right)^{\rho_1\sigma_1\rho_2\sigma_2} \\ & \times\left[g_{\rho_1\sigma_1}g_{\rho_2\sigma_2}z_1z_2 - g_{\rho_1\sigma_1}z_1\frac{4(1-z_2)}{z_2}\hat{k}_{\rho_2}^{\perp 2}\hat{k}_{\sigma_2}^{\perp 2}\right. \\ & \left. - g_{\rho_2\sigma_2}z_2\frac{4(1-z_1)}{z_1}\hat{k}_{\rho_1}^{\perp 1}\hat{k}_{\sigma_1}^{\perp 1} + \frac{4(1-z_1)}{z_1}\hat{k}_{\rho_1}^{\perp 1}\hat{k}_{\sigma_1}^{\perp 1}\frac{4(1-z_2)}{z_2}\hat{k}_{\rho_2}^{\perp 2}\hat{k}_{\sigma_2}^{\perp 2}\right].\end{aligned} \tag{C.12}$$

We have used eq. (C.12) in our implementation of the δNNLO_Γ corrections, since in doing so we have benefitted from the fact that squared amplitudes contracted with an arbitrary four-vector can be obtained by means of `MadNkLO` [20–24].

D Reference frames

The natural reference frame to obtain eq. (3.34) is:

$$F: \quad \text{rest frame of } p_1 + p_2\,, \tag{D.1}$$

which is what has been assumed in appendix B in order to parametrise the four momenta; in particular, we have

$$p_{1,2} = \frac{\sqrt{s}}{2}(1, 0, 0, \pm 1) \tag{D.2}$$

and eq. (B.3)

$$k_j = \frac{\sqrt{s}}{2}\xi_j\left(1, \sqrt{1-y_j^2}\vec{e}_{Tj}, (-)^{j-1}y_j\right) \tag{D.3}$$

for the momenta involved in the collinear splittings of interest.

We also need to consider the c.m. frame of the parton pair that initiates the hard collision — the following is the case where a photon PDF is convoluted on the leg incoming from the left:

$$F_1': \quad \text{rest frame of } z_1p_1 + p_2 \quad \longleftrightarrow \quad \delta(1-y_1)\,, \tag{D.4}$$

JHEP10(2025)224

where the Dirac δ here reminds one that this frame is associated with the collinear configuration $p_1 \parallel k_1$. The boost B_1 from frame F to frame F_1' is given in terms of the boost rapidity η_B. By imposing

$$B_1\left(z_1 p_1 + p_2\right) = \frac{\sqrt{z_1 s}}{2}\left(1,0,0,0\right), \tag{D.5}$$

we obtain

$$\exp(\eta_B) = \sqrt{z_1}\,, \tag{D.6}$$

and we can thus verify that[35]

$$B_1\left(z_1 p_1\right) \equiv \overline{\left(z_1 p_1\right)} = \frac{\sqrt{z_1 s}}{2}\left(1,0,0,1\right), \tag{D.7}$$

$$B_1\left(p_2\right) \equiv \bar{p}_2 = \frac{\sqrt{z_1 s}}{2}\left(1,0,0,-1\right). \tag{D.8}$$

In F_1', we parametrise k_2 as follows:

$$\bar{k}_2 = \frac{\sqrt{z_1 s}}{2}\,\bar{\xi}_2\left(1, \sqrt{1-\bar{y}_2^2}\,\vec{e}_{T2}, -\bar{y}_2\right), \tag{D.9}$$

thus introducing the FKS variables $\bar{\xi}_2$ and $\bar{y}_2$. By equating $\bar{k}_2$ of eq. (D.9) with what we obtain from $B_1(k_2)$ we arrive at:

$$\bar{y}_2 = -\frac{1 - z_1 - y_2(1+z_1)}{1 + z_1 - y_2(1-z_1)}\,, \tag{D.10}$$

$$\bar{\xi}_2 = \frac{\xi_2}{2z_1}\left(1 + z_1 - y_2(1-z_1)\right). \tag{D.11}$$

These variables have the expected properties

$$\xi_2(1-y_2) = z_1\bar{\xi}_2(1-\bar{y}_2)\,, \tag{D.12}$$

$$\xi_2 d\xi_2 dy_2 = z_1\bar{\xi}_2 d\bar{\xi}_2 d\bar{y}_2\,, \tag{D.13}$$

stemming from the invariance of $p_2\cdot k_2$ and $d\phi_1(k_2)$, respectively. One can also verify that the volume of the one-body phase space is correctly computed by the two sets of variables, namely that (see appendix B):

$$\begin{aligned}&\int_{-1}^{1} dy_2 \int d\xi_2\,\xi_2\,\Theta\left(\xi_2 \le \frac{2(z_1 - \hat{M}^2_{\rm INF})}{2-(1+y_2)(1-z_1)}\right)\\ &= z_1\int_{-1}^{1} d\bar{y}_2 \int d\bar{\xi}_2\,\bar{\xi}_2\,\Theta\left(\bar{\xi}_2 \le 1 - \hat{M}^2_{\rm INF}/z_1\right) = z_1\left(1 - \frac{\hat{M}^2_{\rm INF}}{z_1}\right)^2.\end{aligned} \tag{D.14}$$

The upper limit of the ξ_2 integration on the l.h.s. of eq. (D.14) is that of eq. (B.8) in the collinear configuration $y_1 = 1$; that on the $\bar{\xi}_2$ integration is the same one, after y_2 and ξ_2 are given in terms of $\bar{y}_2$ and $\bar{\xi}_2$ by inverting eqs. (D.10) and (D.11). This gives another check of self-consistency, since the upper limit on $\bar{\xi}_2$ is manifestly the correct one for that FKS variable.

[35] Here and elsewhere, boosted momenta will be denoted by means of an overline.

JHEP10(2025)224

The other frame of interest (where a photon PDF is convoluted on the leg incoming from the right) is:

$$F_2' : \quad \text{rest frame of } p_1 + z_2 p_2 \quad \longleftrightarrow \quad \delta(1-y_2)\,. \tag{D.15}$$

The boost from F to F_2' is obtained as before in terms of the boost rapidity:

$$\exp(\eta_B) = 1/\sqrt{z_2}\,. \tag{D.16}$$

The analogue of eq. (D.9) reads:

$$\bar{k}_1 = \frac{\sqrt{z_2 s}}{2}\bar{\xi}_1 \left(1, \sqrt{1-\bar{y}_1^2}\vec{e}_{T1}, \bar{y}_1\right). \tag{D.17}$$

E A distribution identity

Let y be a variable with domain $-1 \le y \le 1$, and $\bar{y}$ a variable with domain $-1 \le \bar{y} \le 1$, which can be related to each other by means of a function g:

$$y = g(\bar{y})\,. \tag{E.1}$$

We assume $g(\bar{y})$ to have the following properties: monotonicity in the whole domain (so that eq. (E.1) constitute a legit change of integration variable $y \leftrightarrow \bar{y}$), and:

$$g(\pm 1) = \pm 1\,, \qquad g(\bar{y}) = 1 - (1-\bar{y})h(\bar{y})\,, \tag{E.2}$$

$$h(\bar{y}) = h_0 + h_1(1-\bar{y}) + \mathcal{O}\left((1-\bar{y})^2\right), \qquad h_0 \neq 0 \tag{E.3}$$

whence

$$h_0 = \frac{dg}{d\bar{y}}(1) > 0\,. \tag{E.4}$$

It is easy to see that the variables $y_{1,2}$ and $\bar{y}_{1,2}$ introduced in appendix D fulfill these conditions.

We use the identity

$$(1-y)^{-1-\epsilon} = -\frac{2^{-\epsilon}}{\epsilon}\,\delta(1-y) + \left(\frac{1}{1-y}\right)_+ + \mathcal{O}(\epsilon). \tag{E.5}$$

In what follows, we shall systematically ignore terms of $\mathcal{O}(\epsilon)$ or higher, since the final result will be obtained in the $\epsilon \to 0$ limit; in keeping with this, the $\mathcal{O}(\epsilon)$ notation will be omitted.

The integral of the y plus distribution (where we omit to denote a test function $f(y)$, which will be understood in the following) is:

$$I = \int dy \left(\frac{1}{1-y}\right)_+ = \int d\bar{y}\frac{dg}{d\bar{y}}\left[(1-\bar{y})^{-1-\epsilon}\left(h(\bar{y})\right)^{-1-\epsilon} + \frac{2^{-\epsilon}}{\epsilon}\,\delta(1-g(\bar{y}))\right], \tag{E.6}$$

where in the r.h.s. we have changed integration variable $y \to \bar{y}$, and expressed all of the dependences on y by means of $g(\bar{y})$. By using again eq. (E.5) we obtain:

$$I = \int d\bar{y}\frac{dg}{d\bar{y}}\left\{\left[-\frac{2^{-\epsilon}}{\epsilon}\,\delta(1-\bar{y}) + \left(\frac{1}{1-\bar{y}}\right)_+\right]\left(h(\bar{y})\right)^{-1-\epsilon} + \frac{2^{-\epsilon}}{\epsilon}\left|\frac{dg}{d\bar{y}}\right|^{-1}\delta(1-\bar{y})\right\}, \tag{E.7}$$

JHEP10(2025)224

whence

$$I = \int d\bar{y} \frac{dg}{d\bar{y}} \left(\frac{1-g(\bar{y})}{1-\bar{y}}\right)^{-1} \left(\frac{1}{1-\bar{y}}\right)_+ + \frac{2^{-\epsilon}}{\epsilon} \int d\bar{y}\, h_0 \Big[- h_0^{-1-\epsilon} + h_0^{-1} \Big] \delta(1-\bar{y})\,. \tag{E.8}$$

Here, we have set $\epsilon = 0$ in the term proportional to the plus distribution (since the result coincides with its finite $\epsilon \to 0$ limit). By expanding in ϵ the coefficients of the terms proportional to the Dirac δ we see that the poles cancel, and we are left with a finite result. Thus we arrive at the sought result:

$$dy \left(\frac{1}{1-y}\right)_+ = d\bar{y} \left\{ \frac{dg}{d\bar{y}} \left(\frac{1-g(\bar{y})}{1-\bar{y}}\right)^{-1} \left(\frac{1}{1-\bar{y}}\right)_+ + \log h_0\, \delta(1-\bar{y}) \right\}. \tag{E.9}$$

Equation (E.9) can be further manipulated by employing the identity of eq. (5.15) on the plus distributions on the two sides, introducing two arbitrary parameters $\delta_{\rm I}$ and $\bar{\delta}_{\rm I}$ to control the endpoint subtraction in the y and $\bar{y}$ variable, respectively. In this way:

$$dy \left(\frac{1}{1-y}\right)_{\delta_{\rm I}} = d\bar{y} \left\{ \frac{dg}{d\bar{y}} \left(\frac{1-g(\bar{y})}{1-\bar{y}}\right)^{-1} \left(\frac{1}{1-\bar{y}}\right)_{\bar{\delta}_{\rm I}} + \log \frac{h_0 \bar{\delta}_{\rm I}}{\delta_{\rm I}}\, \delta(1-\bar{y}) \right\}. \tag{E.10}$$

We can apply eq. (E.10) to the $(y_2, \bar{y}_2)$ pair of variables we have used in frame F_1', and to the pair $(y_1, \bar{y}_1)$ relevant to frame F_2'. A simple algebra leads to:

$$dy_2 \left(\frac{1}{1-y_2}\right)_{\delta_{\rm I}} = d\bar{y}_2 \left\{ \left(\frac{d\xi_2}{d\bar{\xi}_2}\right)^{-1} \left(\frac{1}{1-\bar{y}_2}\right)_{\bar{\delta}_{\rm I}} + \log \frac{z_1 \bar{\delta}_{\rm I}}{\delta_{\rm I}}\, \delta(1-\bar{y}_2) \right\}, \tag{E.11}$$

$$dy_1 \left(\frac{1}{1-y_1}\right)_{\delta_{\rm I}} = d\bar{y}_1 \left\{ \left(\frac{d\xi_1}{d\bar{\xi}_1}\right)^{-1} \left(\frac{1}{1-\bar{y}_1}\right)_{\bar{\delta}_{\rm I}} + \log \frac{z_1 \bar{\delta}_{\rm I}}{\delta_{\rm I}}\, \delta(1-\bar{y}_1) \right\}. \tag{E.12}$$

F Factorisation scheme at the LL

We begin this discussion by reminding the reader that while at this order the scheme is not a factorisation scheme, it has been shown in appendix A of ref. [12] how K_{ij} functions may be introduced here as well, as compensating factors which correct for the fact that the first-order coefficients in the expansion of the PDFs do not coincide with the correct results computed in ref. [8]. However, it is crucial to bear in mind that such compensating factors are *solely* associated with $\mathcal{O}(\alpha^{b+1})$ cross sections, and not with PDFs. In other words, the relevant K_{ij} functions must only be included in the $(n+1)$-body degenerate contributions to $d\hat{\sigma}^{[1]}$ (and, by extension, to their analogues at higher orders), and not in the expansions of the PDFs, where they simply do not appear. In the present context, by construction $\mathcal{Q}'_{\gamma\ell}$, $d\delta^{[1]}$, $d\delta_D^{[2]}$, and $d\delta_S^{[2]}$ are matrix-level quantities and, therefore, must feature the LL K_{ij} functions introduced above. For example, this is the only way in which eq. (5.25) can be fulfilled.

In order to be more definite, we report some explicit results relevant to the LL PDFs. We limit ourselves to considering the so-called collinear and running schemes, introduced in ref. [5],

JHEP10(2025)224

since in the standard ones (namely, beta, eta, and mixed) the photon is equal to zero. For the quantities we are interested in, the collinear and running scheme results coincide. We have:

$$\Gamma_{\ell/\ell}(z) = \delta(1-z) + \frac{\alpha}{2\pi}\left(\frac{1+z^2}{1-z}\right)_+ \log\frac{\mu^2}{\mu_0^2} + \mathcal{O}(\alpha^2)\,, \tag{F.1}$$

$$\Gamma_{\gamma/\ell}(z) = \frac{\alpha}{2\pi}\,\frac{1+(1-z)^2}{z}\,\log\frac{\mu^2}{\mu_0^2} + \mathcal{O}(\alpha^2)\,. \tag{F.2}$$

The $\mathcal{O}(\alpha)$ coefficients above can be compared to their NLL-PDF counterparts in eq. (**I**.4.121) and eq. (**I**.4.189) (eq. (3.28) here). Note that at $\mathcal{O}(\alpha)$ the LL PDFs depend on the starting scale μ_0; such a dependence drops out at the NLL (in practice, however, there is no good reason to choose $\mu_0 \neq m$). The compensating $K_{\ell\ell}$ function stemming from eq. (F.1) are given in appendix A of ref. [12], and will not be repeated here. The one stemming from eq. (F.2) is:

$$K_{\gamma\ell} = \frac{1+(1-z)^2}{z}\left(2\log z + 1 - \log\frac{\mu_0^2}{m^2}\right). \tag{F.3}$$

By means of explicit calculations we can verify that:

$$\text{eq. (3.28)}\big[K_{\gamma\ell}(z) = \text{eq. (F.3)}\big] = \frac{2\pi}{\alpha} \times \text{eq. (F.2)}\,, \tag{F.4}$$

and:

$$\mathcal{Q}'_{\gamma\ell}(z)\big[K_{\gamma\ell}(z) = \text{eq. (F.3)}\big] + \frac{2\pi}{\alpha} \times \text{eq. (F.2)} = \mathcal{Q}_{\gamma\ell}(z)\,. \tag{F.5}$$

Data Availability Statement. This article has no associated data or the data will not be deposited.

Code Availability Statement. This article has no associated code or the code will not be deposited.

References

[1] S. Frixione et al., *Initial state QED radiation aspects for future e^+e^- colliders*, in the proceedings of the *Snowmass 2021*, Seattle, U.S.A., July 17–26 (2022) [arXiv:2203.12557] [INSPIRE].

[2] S. Frixione, F. Maltoni, D. Pagani and M. Zaro, *Precision phenomenology at multi-TeV muon colliders*, *JHEP* **09** (2025) 036 [arXiv:2506.10733] [INSPIRE].

[3] T. Han, Y. Ma and K. Xie, *High energy leptonic collisions and electroweak parton distribution functions*, *Phys. Rev. D* **103** (2021) L031301 [arXiv:2007.14300] [INSPIRE].

[4] F. Garosi, D. Marzocca and S. Trifinopoulos, *LePDF: Standard Model PDFs for high-energy lepton colliders*, *JHEP* **09** (2023) 107 [arXiv:2303.16964] [INSPIRE].

[5] V. Bertone, M. Cacciari, S. Frixione and G. Stagnitto, *The partonic structure of the electron at the next-to-leading logarithmic accuracy in QED*, *JHEP* **03** (2020) 135 [*Erratum ibid.* **08** (2022) 108] [arXiv:1911.12040] [INSPIRE].

JHEP10(2025)224

[6] S. Frixione and G. Stagnitto, *The muon parton distribution functions*, *JHEP* **12** (2023) 170 [arXiv:2309.07516] [INSPIRE].

[7] M. Bonvini, S. Frixione and G. Stagnitto, *Improved small-x resummation for DGLAP splitting functions: HELL 4.0*, in preparation.

[8] S. Frixione, *Initial conditions for electron and photon structure and fragmentation functions*, *JHEP* **11** (2019) 158 [arXiv:1909.03886] [INSPIRE].

[9] S. Frixione, Z. Kunszt and A. Signer, *Three jet cross-sections to next-to-leading order*, *Nucl. Phys. B* **467** (1996) 399 [hep-ph/9512328] [INSPIRE].

[10] S. Frixione, *A general approach to jet cross-sections in QCD*, *Nucl. Phys. B* **507** (1997) 295 [hep-ph/9706545] [INSPIRE].

[11] S. Frixione, *On factorisation schemes for the electron parton distribution functions in QED*, *JHEP* **07** (2021) 180 [*Erratum ibid.* **12** (2012) 196] [arXiv:2105.06688] [INSPIRE].

[12] V. Bertone et al., *Improving methods and predictions at high-energy e^+e^- colliders within collinear factorisation*, *JHEP* **10** (2022) 089 [arXiv:2207.03265] [INSPIRE].

[13] R. Frederix, S. Frixione, F. Maltoni and T. Stelzer, *Automation of next-to-leading order computations in QCD: The FKS subtraction*, *JHEP* **10** (2009) 003 [arXiv:0908.4272] [INSPIRE].

[14] S. Frixione, M.L. Mangano, P. Nason and G. Ridolfi, *Improving the Weizsacker-Williams approximation in electron-proton collisions*, *Phys. Lett. B* **319** (1993) 339 [hep-ph/9310350] [INSPIRE].

[15] J. Alwall et al., *The automated computation of tree-level and next-to-leading order differential cross sections, and their matching to parton shower simulations*, *JHEP* **07** (2014) 079 [arXiv:1405.0301] [INSPIRE].

[16] R. Frederix et al., *The automation of next-to-leading order electroweak calculations*, *JHEP* **11** (2018) 085 [*Erratum ibid.* **11** (2021) 085] [arXiv:1804.10017] [INSPIRE].

[17] A. Sirlin, *Radiative Corrections in the $SU(2)_L \times U(1)$ Theory: A Simple Renormalization Framework*, *Phys. Rev. D* **22** (1980) 971 [INSPIRE].

[18] W.A. Bardeen, A.J. Buras, D.W. Duke and T. Muta, *Deep Inelastic Scattering Beyond the Leading Order in Asymptotically Free Gauge Theories*, *Phys. Rev. D* **18** (1978) 3998 [INSPIRE].

[19] S. Catani and M.H. Seymour, *A general algorithm for calculating jet cross-sections in NLO QCD*, *Nucl. Phys. B* **485** (1997) 291 [hep-ph/9605323] [INSPIRE].

[20] S. Lionetti, *Subtraction of Infrared Singularities at Higher Orders in QCD*, Ph.D. thesis, Eidgenössische Technische Hochschule (ETH), CH-8092 Zürich, Switzerland (2018) [INSPIRE].

[21] V. Hirschi, S. Lionetti and A. Schweitzer, *One-loop weak corrections to Higgs production*, *JHEP* **05** (2019) 002 [arXiv:1902.10167] [INSPIRE].

[22] M. Becchetti et al., *Next-to-leading order corrections to light-quark mixed QCD-EW contributions to Higgs boson production*, *Phys. Rev. D* **103** (2021) 054037 [arXiv:2010.09451] [INSPIRE].

[23] R. Bonciani et al., *Next-to-leading-order QCD corrections to Higgs production in association with a jet*, *Phys. Lett. B* **843** (2023) 137995 [arXiv:2206.10490] [INSPIRE].

[24] G. Bertolotti, P. Torrielli, S. Uccirati and M. Zaro, *Local analytic sector subtraction for initial- and final-state radiation at NLO in massless QCD*, *JHEP* **12** (2022) 042 [arXiv:2209.09123] [INSPIRE].

JHEP10(2025)224